POLITECHNIKA KRAKOWSKA im. T. Kościuszki
Wydział Mechaniczny
Instytut Technologii Maszyn i Automatyzacji Produkcji

Kierunek studiów: Automatyka i Robotyka
Specjalność: Technologie Informacyjne w Systemach Produkcyjnych

STUDIA STACJONARNE

PRACA DYPLOMOWA

MAGISTERSKA

Marek Gutt-Mostowy

CO_2 FLEXIBLE VACUUM INSULATED TRANSFER LINE FOR ATLAS IBL DETECTOR COOLING SYSTEM

ELASTYCZNA LINIA PRZESYŁOWA DWUTLENKU WĘGLA IZOLOWANA PRÓŻNIĄ DLA SYSTEMU CHŁODNICZEGO DETEKTORA IBL EKSPERYMENTU ATLAS

Promotor:
Prof. dr hab. inż. Piotr Cyklis

Kraków, rok akad. 2012/2013

CERN-THESIS-2013-371
26/11/2013

Autor pracy: Marek Gutt-Mostowy

Nr pracy: ……

OŚWIADCZENIE O SAMODZIELNYM WYKONANIU PRACY DYPLOMOWEJ

Oświadczam, że przedkładana przeze mnie praca dyplomowa magisterska/inżynierska* została napisana przeze mnie samodzielnie. Jednocześnie oświadczam, że ww. praca:

1) nie narusza praw autorskich w rozumieniu ustawy z dnia 4 lutego 1994 r. o prawie autorskim i prawach pokrewnych (Dz.U. z 2006 r. Nr 90, poz. 631 z późn. zm.) oraz dóbr osobistych chronionych prawem cywilnym, a także nie zawiera danych i informacji, które uzyskałem/am* w sposób niedozwolony,

2) nie była wcześniej podstawą żadnej innej procedury związanej z nadawaniem tytułów zawodowych, stopni lub tytułów naukowych.

Jednocześnie przyjmuję do wiadomości, że w przypadku stwierdzenia popełnienia przeze mnie czynu polegającego na przypisaniu sobie autorstwa istotnego fragmentu lub innych elementów cudzej pracy, lub ustalenia naukowego, właściwy organ stwierdzi nieważność postępowania w sprawie nadania mi tytułu zawodowego (art. 193 ustawy z dnia 27 lipca 2005 r. Prawo o szkolnictwie wyższym, Dz.U. z 2012 r. poz. 572).

……
data i podpis

* niepotrzebne skreślić

Uzgodniona ocena pracy: ……..

……	.....	.....
podpis promotora	podpis recenzenta	podpis dyrektora instytutu ds. dydaktyki

Table of Contents

1 Summary **7**

2 Introduction **9**

3 Thesis objectives and scope **12**

3.1 Educational objective 12

3.2 Practical objective 12

3.3 Thesis scope 12

4 Literature review **13**

5 Design of the transfer line **15**

5.1 Inner pipe 16

5.2 Multi-layer insulation 16

5.3 Spacer 17

5.4 Flexible hose and rigid tube 18

6 Experimental setup **19**

6.1 Data Acquisition System 19

6.1.1 Multimeter 19

6.1.2 Current source 20

6.1.3 Temperature sensors 20

6.1.4 Mass flow meter 22

6.1.5 Vacuum gauge 23

6.1.6 LabVIEW program 24

6.1.7 Measurement accuracy 24

6.2 Peripheral devices 25

6.2.1 Chiller 25

6.2.2 Vacuum pump 27

6.2.3 IR camera 28

6.3 Measurement configurations 28

6.3.1 Straight configuration 30

6.3.2 Coiled tight/relaxed configuration 32

6.3.3 Bent rigid part of the transfer line 33

7 Results **35**

7.1 Straight configuration 35

7.1.1 Measurements with different mass flow rates 36

7.1.2 Measurements at different coolant temperatures 39

7.1.3 Measurements at different vacuum pressures 42

7.2 Coiled tight/relaxed configuration 45

7.3 Bent rigid part of the transfer line 49

8 Conclusions **52**

Appendices **54**

List of references..... 63

1 Summary

CERN is a leading international nuclear research centre, which servers 10000 scientists from 85 different countries. Thanks to its large particle accelerator complex it has contributed to major discoveries in physics in recent years.

ATLAS is one of the experiments of the Large Hadron Collider, which enabled particle physicists to tentatively confirm existence of the long predicted Higgs boson. After the first operation period LHC and its experiments are currently undergoing maintenance and upgrade works, which began in February 2013.

One of the major improvements in tracking robustness and precision in ATLAS experiment is expected due to the installation of the new Insertable B-Layer detector. Strong constrains and project specifications led to the decision of using CO_2 as a refrigerant for detector cooling, which is more efficient in terms of pipe dimensions and mass flow.

During the design of the piping routing for the cooling system it was found out that there is not enough room at the Inner Detector Endplate for the CO_2 transfer line with its standard foam insulation Armaflex. In order to reduce the transfer line bundle outer diameter it was decided to use vacuum as insulation. However, no commercial systems existed for CO_2 flexible vacuum insulated transfer lines. As a result, an experimental project has been launched by the Cryolab and Instrumentation section in co-operation with the Detector Infrastructure section aimed at researching and developing feasible solution to the encountered problem.

Studies on vacuum insulation technologies conducted by Dr Thomas Eisel resulted in a design of CO_2 flexible vacuum insulated transfer line. A short length mock-up of the proposed transfer line was built and tested in straight and coiled configuration. This early trial provided promising outlook on the technology and it was decided to setup a new experiment with a close to full-scale transfer line. The results of this experiment are presented in Chapter 7 of this thesis.

The new mock-up consisted of an inner tube with a total length of 9.8 m and an outer rigid pipe welded at one end to a corrugated flexible hose. The last two elements formed together the outermost layer of the transfer line. Additionally, the inner tube was covered with Multi-Layer Insulation and a glass fibre spacer placed in the vacuum interspace. A detailed description of the transfer line design is presented in Chapter 5 of this thesis.

A Data Acquisition System was created especially for the purpose of the experiment in a LabVIEW environment. Multiple sensors were used including mass flow meter, vacuum gauge and temperature sensors. Moreover, an overall temperature distribution on the surface of the transfer line was observed using infrared camera.

The measurements were performed in three different configurations of the transfer line in accordance with the IBL Cooling System project specifications. This included testing of the performance of the transfer line in straight, coiled – tight and coiled – relaxed configurations. Furthermore, one additional set of measurements was performed for the coiled – relaxed configuration with the bent rigid pipe of the transfer line at a 90° angle.

All the tests were performed at two different vacuum pressures. The only exception is the straight configuration, where additionally performance of the transfer line was measured with

different mass flow rates and at different coolant temperatures. Chapter 6 of this thesis is devoted to a detailed description of the experimental setup.

The conducted research provides positive results on the thermal performance of the transfer line. As expected the results in straight configuration delivered the lowest values of temperature differences between ambient and surface temperatures as well as the lowest heat transfer rate values from ambient to the coolant.

Although temperature difference values between ambient and surface temperatures in coiled - tight and coiled - relaxed configurations greatly exceeded those in straight configuration, they are still within a safety margin from the critical point where condensation would occur on the surface of the transfer line in the ATLAS experiment cavern.

As a result in Chapter 8 of the thesis it is concluded that the investigated transfer line can be safely used for the ATLAS IBL Detector Cooling System.

2 Introduction

CERN is a leading particle physics laboratory. Having 59 years of history (2013) it has grown to the biggest nuclear research centre in the world. It was founded by 12 member states. By 2013 the number of the member states increased to 21.

CERN is located on the Swiss-French border in the Geneva region and employs 2500 staff. Additionally, it serves 10000 scientists from all over the world representing 580 universities and 85 different nationalities [1].

Over the years several major achievements in particle physics have been reached due to the experiments concluded at CERN. In 1983 the W and Z bosons were discovered thanks to the UA1 and UA2 experiments. In 1995 for the first time antihydrogen atoms were created in the PS210 experiment, followed by further experiments with antimatter. As a result in 2011 antihydrogen was created and maintained for over 15 minutes.

Recently CERN became well known for its contribution to the discovery of Higgs boson. The existence of the particle long predicted by theoretical models of Peter Higgs and François Englert was confirmed independently by the two largest experiments at CERN – CMS and ATLAS. After the results of the experiments were published in 2012 Peter Higgs and François Englert were jointly awarded Noble Prize in physics in 2013.

The mentioned discoveries were possible due to the large complex of particle accelerators among which LHC is the newest and the biggest one. LHC has 27 km circumference and is located 100 m underground. The particles inside of the accelerator reach energy level of 7 TeV and travel nearly at the speed of light to be then collided. The observations of the particles created in these interactions lead to new discoveries in physics.

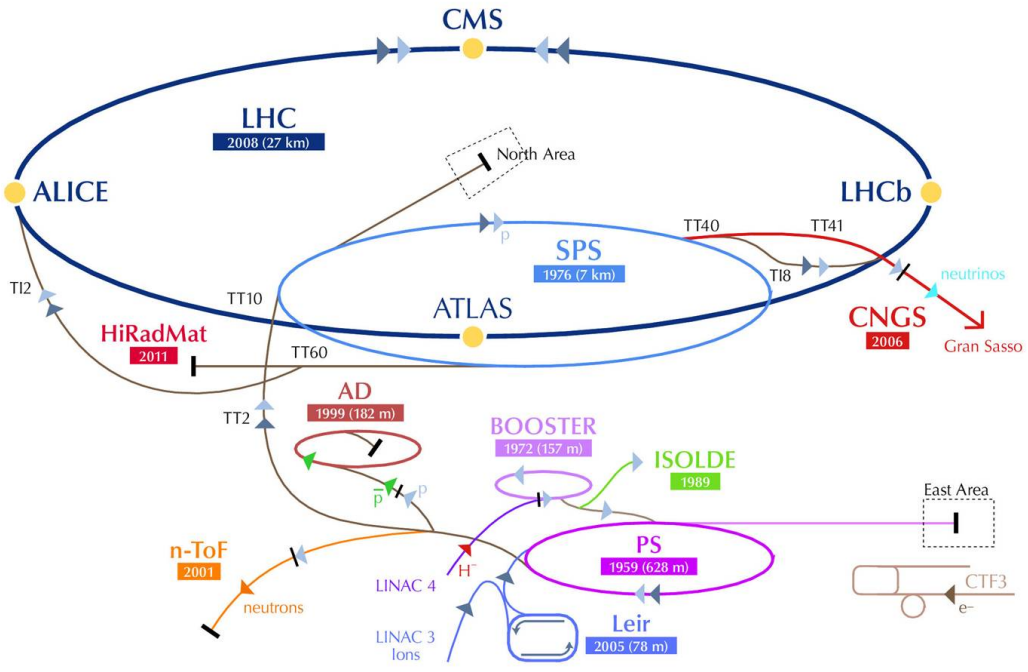


Figure 2-1 Schematic of CERN accelerator complex with four experiments on LHC **[1]**.

After some years of operation LHC and its experiments are undergoing maintenance and upgrade work. One of the major improvements in tracking robustness and precision in ATLAS experiment is expected thanks to the installation of the new Insertable B-Layer detector. CO_2 was chosen as a coolant for the detector infrastructure during its normal operation and during the bake-out [2].

Due to the space constrains near the detector in ATLAS experiment it was not possible to use standard insulation material for the CO_2 transfer lines - Armaflex. In some parts of the transfer line the thickness including its insulation could not exceed 14 mm. Moreover, the transfer line had to remain flexible in order to facilitate the installation process. There were no commercial products available on the market, which would meet the above-mentioned criteria. Therefore, it was decided to research and develop a flexible vacuum insulated transfer line. This thesis describes the experiment conducted in order to verify if the proposed design of the transfer line can be used in the final application.

Figure 2-2 shows the Piping & Instrumentation Diagram of the IBL CO_2 cooling transfer and evaporator system. The part of the transfer line of interest is located between Muon Sector 5 and Dry volume with the detector. This area of the ATLAS experiment contains air. Therefore, in order to avoid condensation, temperatures lower than 10°C degrees must be avoided.

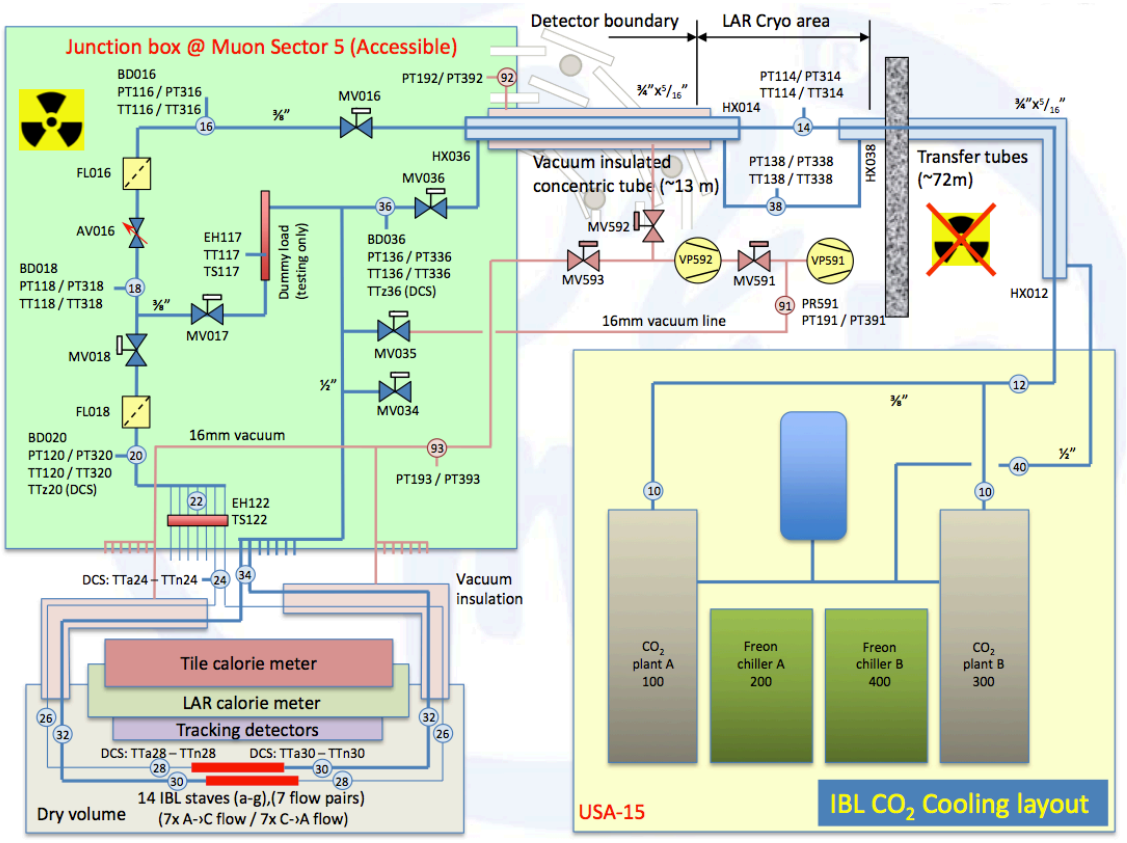


Figure 2-2 P&I of the IBL CO_2 cooling transfer and evaporator system **[3]**.

Figure 2-3 presents side view of the Inner Detector Endplate with the proposed routing of the flexible vacuum insulated transfer line. The transfer line consists of two parts – stiff and flexible, both of which need to be bended. The stiff tube will be subjected to bending twice at a

45 degrees angle, whereas the flexible will be bended at least once at a 90 degrees angle, however, with a bigger radius.

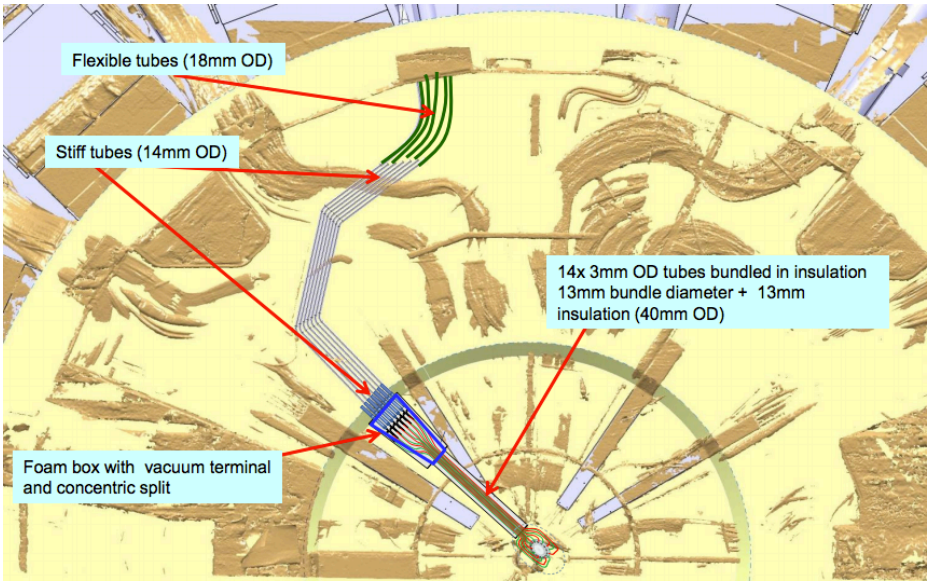


Figure 2-3 Routing of the transfer lines at side A of Inner Detector Endplate. **[4]**

The Experiment, which is the subject of this thesis, was preceded by the the short section test of the transfer line, conducted by Dr Thomas Eisel and Carlos Arregui in Cryolab and Instrumentation section at CERN. Their positive results led to further research with close to full-scale mock-up, made in collaboration with the Detector Infrastructure group of the Physics Department at CERN.

3 Thesis objectives and scope

3.1 Educational objective

The main educational objective of this thesis is to study basic thermodynamic concepts connected with heat transfer, as well as to acquire techniques used in data acquisition systems and data analysis.

3.2 Practical objective

The practical objective of this thesis is to determine if the proposed design of the flexible vacuum insulated CO_2 transfer line can be used for the ATLAS IBL Detector Cooling System. Moreover, it aims to present manufacturing procedures of the transfer line in great detail in order to facilitate the production of such a line in the future.

3.3 Thesis scope

The experiment, which results are presented and discussed in this thesis, was performed during the Long Shut Down 1 of LHC at CERN in 2013. It was motivated by the lack of a commercial solution of flexible vacuum insulated transfer lines for CO_2, which were required for the ATLAS IBL detector cooling system. The research is based on studies of similar solutions used in cryogenic applications and the analysis of obtained results representing performance of the transfer line under different conditions and in different configurations.

4 Literature review

Vacuum as an insulator of transfer lines is widely used in cryogenics applications in order to minimize the heat inleak from the environment, as it reduces heat transfer by convection [5]. It is normally used in connection with insulating materials like Multi-Layer Insulation (MLI) to reduce heat loss by thermal radiation and specific types of spacing materials that minimize the surface area of the inner tube of the transfer line that remains in contact with the outer tube of the transfer line. As a result the heat transfer by conduction is minimized.

Vacuum insulated transfer lines are being studied at different vacuum levels as in [6] or for specific cases like under a sudden loss of insulating vacuum in [7]. All of the results show poor insulating properties in soft vacuum or no vacuum. Specific materials are being developed like Layered Composite Insulation (LCI) that show better insulating properties without the presence of high vacuum in comparison to MLI [8]. However, their performance is not yet at a level that would meet the typical requirements, which often mean good insulating properties in space as well as on earth.

A typical design of the transfer line using vacuum as an insulator is presented in Figure 4-1. The inner pipe with the coolant is inside of a vacuum chamber. Spacing materials is situated at the ends of the straight parts of the transfer line, as otherwise the inner pipe would touch the outer pipe. The cross-section of spacer piece demonstrates that it is of triangular shape. As a result only the apexes touch the outer hose, reducing the contact surface as much as possible.

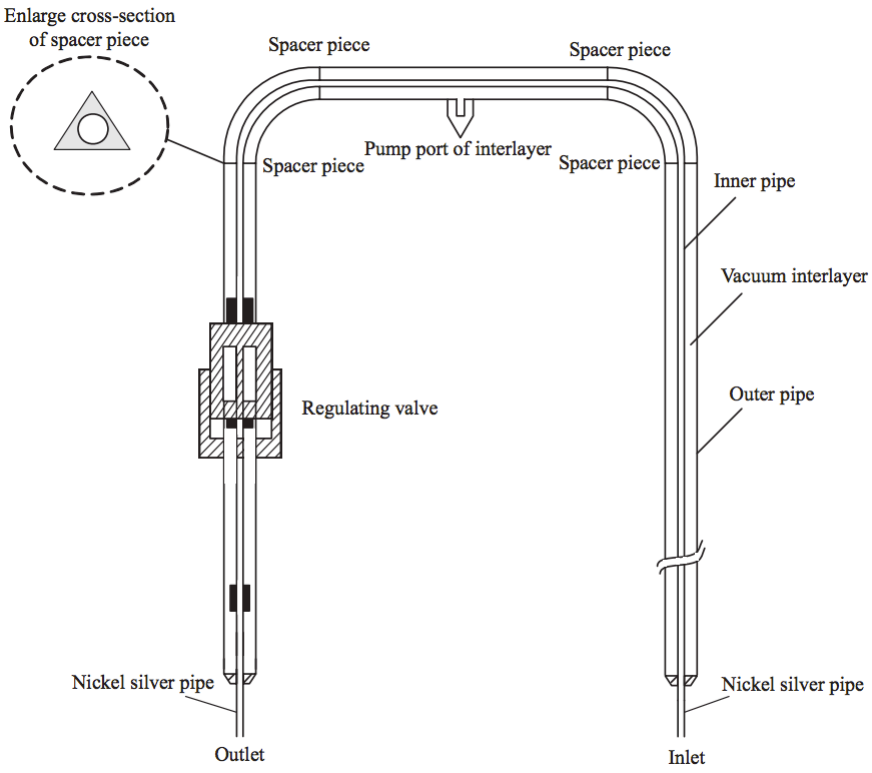


Figure 4-1 Components of a cryogenic transfer line **[5]**.

Due to the recently increased interest in superconducting technologies more studies have been performed on vacuum insulated transfer lines that could be bendable [6]. They are mostly used for High Temperature Superconducting (HTS) Cables [17]. Successful pilot projects among few is described in [9] and led to further development in [10].

As a result spacing material concepts have been developed. One of them is a spiral spacer that separates the inner tube from the outer one on the whole length of the transfer line [11]. Other solutions include several layers of spiral spacers with extremely low heat conductance with multiple contact points between inner and outer tube.

Long flexible transfer lines have been additionally studied for distributed cryogenic systems used for cooldown and warmup of superconducting magnets [12]. In this case gaseous and liquid helium is used with positive results.

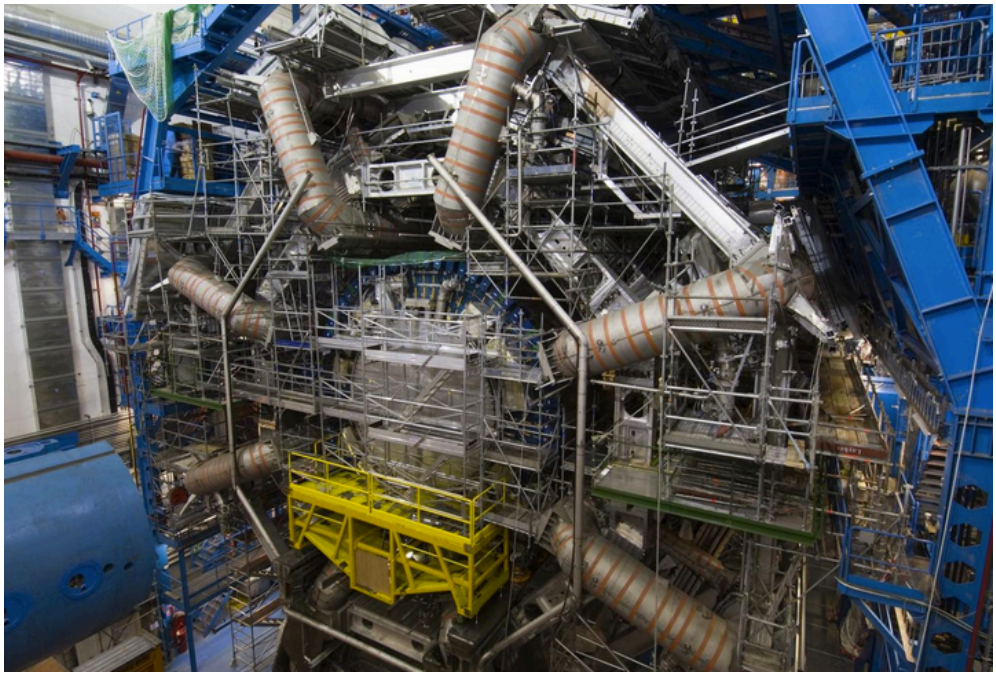


Figure 4-2 Superconducting magnets in ATLAS experiment arranged in a torus **[1]**.

None of the research, however, was performed on flexible vacuum insulated transfer lines with CO_2 acting as a coolant. All of the transfer lines used for transportation of liquid helium or nitrogen have diameters greatly exceeding those used for CO_2 in detector cooling systems [13] [14]. Therefore, it is difficult to predict its thermal performance.

As a result the study presented in this thesis needed to be conducted.

5 Design of the transfer line

This chapter presents the design of the transfer line that has been proposed by Dr Thomas Eisel as the basis for the mock-up of the transfer line developed for the purposes of this experiment. A figurative description of the transfer line is presented and followed by an explanation of the design choices with respect to the final requirements of the ATLAS experiment [15].

Each element used to build the transfer line is described in detail. Additionally, the assembly procedure is explained with an emphasis on the sewing of the MLI, a technique which can be used in the production of future transfer lines.

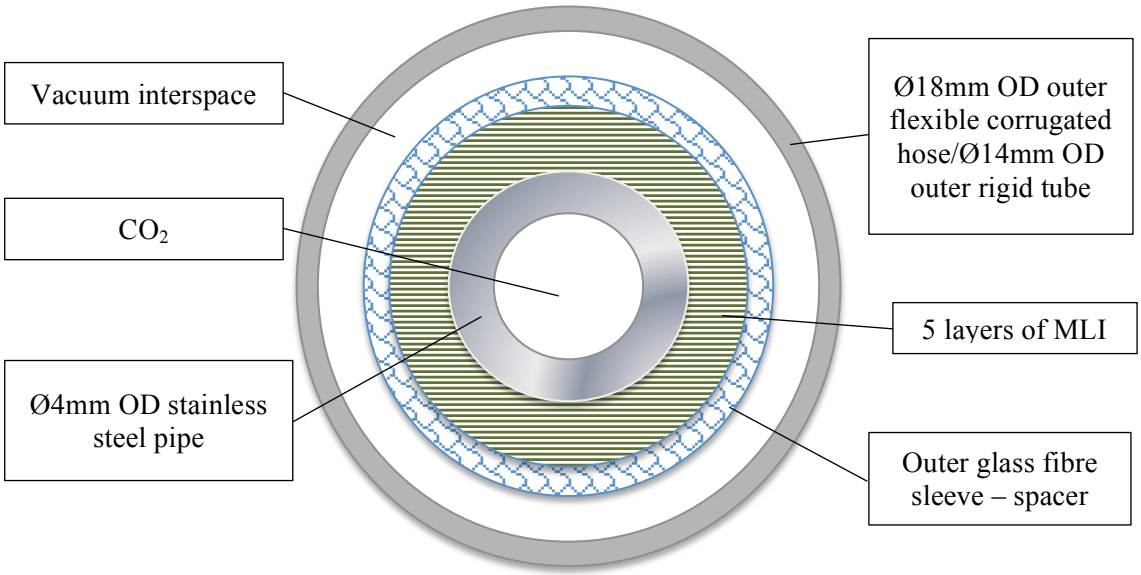


Figure 5-1 Design of the transfer line.

Figure 5-1 presents the design of the transfer line, based on which the experimental setup was built. The most centric element is a stainless steel pipe of 4 mm outside diameter. It is the pipe that is used for the coolant transport.

The second layer from the centre, which is filled with stripes, is the MLI. It is used to avoid heat transfer by radiation. Five layers of the MLI are used; separated by a non-woven spacer.

The third layer is the glass fibre sleeve used to limit conduction between the inner pipe of the transfer line and the outer hose or the pipe. It acts as a continuous spacer to the inner pipe and becomes a crucial element in particular during the process of bending of the transfer line.

The last layer is a flexible stainless still corrugated hose, which has a 18 mm outside diameter or a rigid tube made out of stainless steel, which has a 14 mm outside diameter. The material used for the last layer depends on the part of the transfer line. The overall view is available in Figure 6-15.

Between the inner stainless steel pipe and the outer stainless still pipe or flexible hose there is a vacuum, which aims at eliminating heat transfer by convection.

5.1 Inner pipe

For the purposes of this experiment a mechanical model of the experiment setup was created. As a result the proper length of the inner pipe was calculated that facilitated the process of connection of the Swagelok parts at the end of the transfer line. The space available for the wrenches once the steel bellows were squeezed was very limited, therefore, the pipe length had to be precisely calculated. The Figure 5-2 shows the inner pipe after welding and pressure test in the laboratory. The pipe was prepared out of 6 m long sections and has a length of 9801 mm.

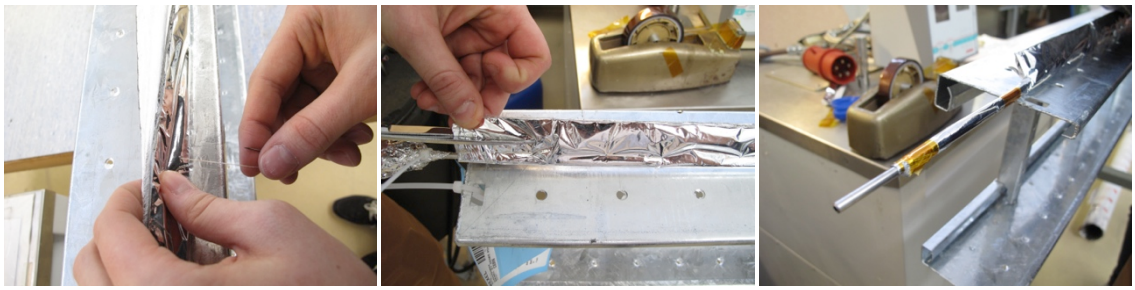


Figure 5-2 Inner pipe of the transfer line.

5.2 Multi-layer insulation

The inner pipe of the transfer line was covered with the MLI, which reduces heat transfer by radiation and conduction. Figure 5-3 presents process of the MLI installation. Firstly, the delivered MLI had to be divided into pieces each consisting of 5 layers. Otherwise, the pipe with the MLI would become too thick for the glass fibre spacer. Secondly, the insulation was wrapped around the inner pipe and sewn using running stitch technique. As an effect, the stitches were approximately 5 cm long. It is essential to retain this length of the stitches as otherwise if sewn too dense MLI might break during the bending of the transfer line. One has to be careful also with the strength applied to create stitches, Should the stitches be sewn too tightly the MLI might break while bending of the transfer line.

Once the MLI was sewn it was necessary to cut off the excess of the material. This procedure was followed by the taping of the MLI with Kapton tape. In consequence, the MLI stuck to the inner pipe and could be covered with the glass fibre spacer. The result of this process can be observed on Figure 5-3c.



a **b** **c**

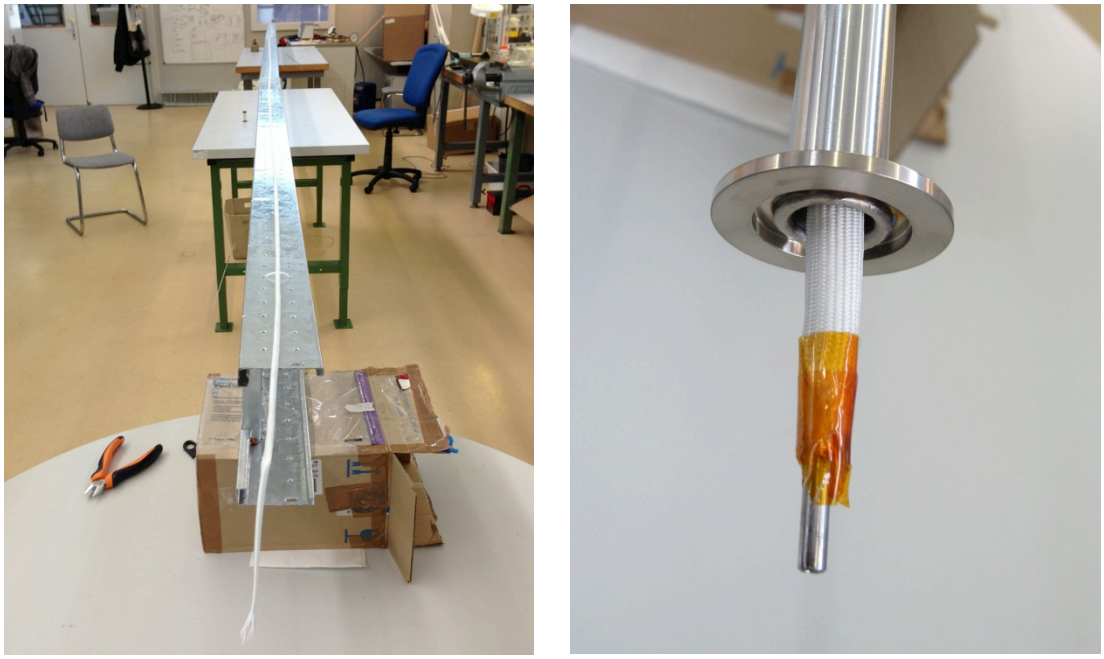
Figure 5-3 Process of the multi-layer insulation installation; a) sewing of the MLI; b) cutting off the excess of the MLI; c) MLI taped with Kapton tape;

5.3 Spacer

In order to additionally limit heat transfer by conduction of the inner pipe to the outer, it was necessary to pull a spacer made out of glass fibre over the inner pipe with MLI wrapped around it. This element becomes of a particular importance during the process of bending of the transfer line when the distance between the inner pipe and the outer hose or tube is greatly reduced.

One of the initial ideas was to use springs that would prevent the direct contact between the inner pipe and the outer hose or pipe. However, due to the ability of the glass fibre spacer to cover the entire surface of the inner pipe, it was decided to implement this spacer solution.

Figure 5-4a presents the spacer sleeve pulled over the entire length of the inner tube, whereas Figure 5-4b shows the very end which was attached with Kapton tape to the inner pipe in order to prevent movement of the spacer.



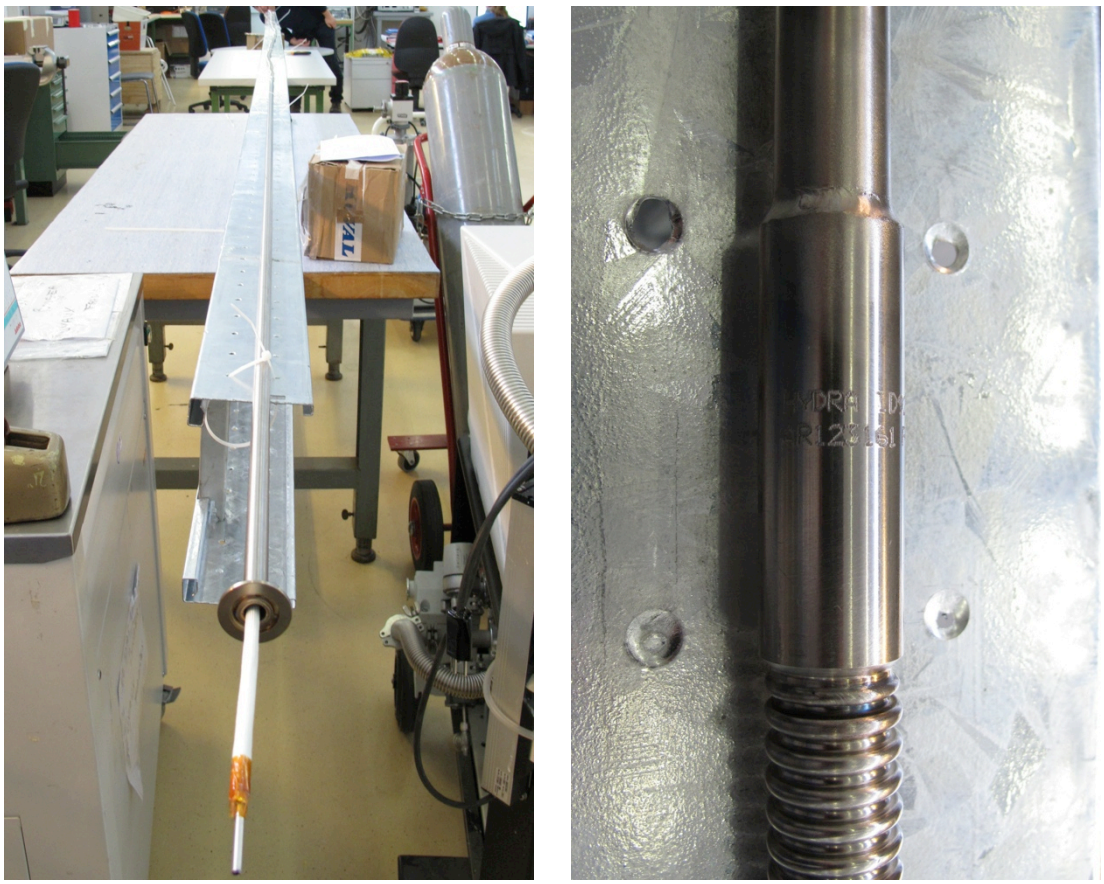
a **b**

Figure 5-4 Inner tube with MLI and the spacer; a) spacer pulled over the entire length of the inner tube; b) end of the inner tube with MLI and the spacer

5.4 Flexible hose and rigid tube

Once all the insulation materials were in place the outer flexible hose welded together with the rigid pipe was slid on. The flexible corrugated hose was 7 m long; the remainder was the rigid pipe with length of 2.5 m.

Figure 5-5a presents the assembled transfer line. In the Figure 5-5b the weld between corrugated hose and the rigid pipe can be observed in detail.



a **b**

Figure 5-5 Rigid tube and flexible hose of the transfer line; a) Rigid tube with vacuum flange over the inner tube with the MLI and the spacer; b) welded connection between the rigid tube and the flexible hose

6 Experimental setup

This chapter presents the Data Acquisition System (DAQ) created for the purposes of this experiment and describes the measurement configurations in which the read-out of the data was performed. Additionally, peripheral devices are presented to give a general overview on the equipment used.

The subchapter devoted to the DAQ deals with the devices and measurement techniques that were used to gather the data. It aims at providing the accuracies of measurements to estimate the error in the final results. The last part of this subchapter presents the main screen of the graphical user interface of the LabVIEW program in order to explain the workflow during the measurements.

The peripheral devices subchapter in addition to the main description part deliberates on the extra procedures performed before the start of the measurements.

6.1 Data Acquisition System

This subchapter presents all the measuring devices used in the experiment as well as informs the reader about their accuracies.

6.1.1 Multimeter

For the read-out of the data the Keithley 2000 multimeter was used connected to a laptop running Windows by GPIB-USB-HS connector. The multimeter had additional scanning card installed to serve up to 10 channels.



a **b**

Figure 6-1 a) Keithley 2000 multimeter; b) GPIB-USB connector;

The voltage was measured in range of 100 mV. For this range the resolution of the multimeter is equal to 0.1 μV.

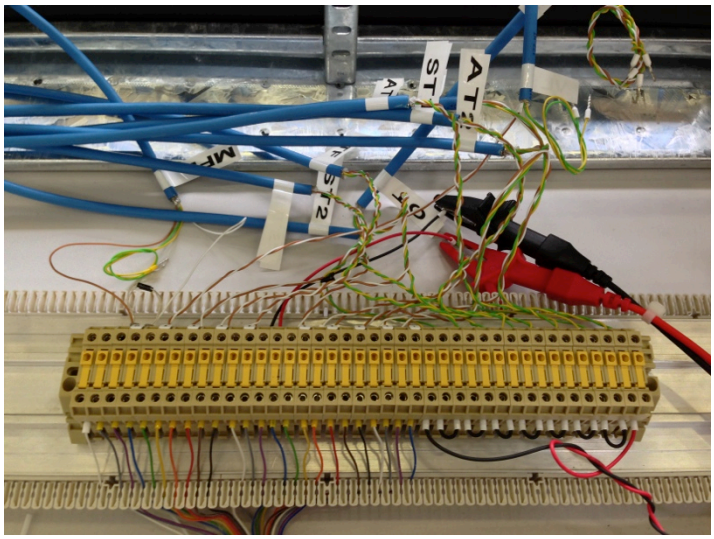


Figure 6-2 Terminals connecting cables from sensors with multimeter.

Due to the fact that the experimental setup had to be moved few times during the measurements the terminals were prepared on the DIN rail in order to facilitate the connection of cables.

6.1.2 Current source

Measurements of the temperatures were performed using 4-wire sensing technique. For the sensors excitation the LakeShore DC source was employed. Sensor excitation was set to 1mA. Below that value there was too much noise in the signal.

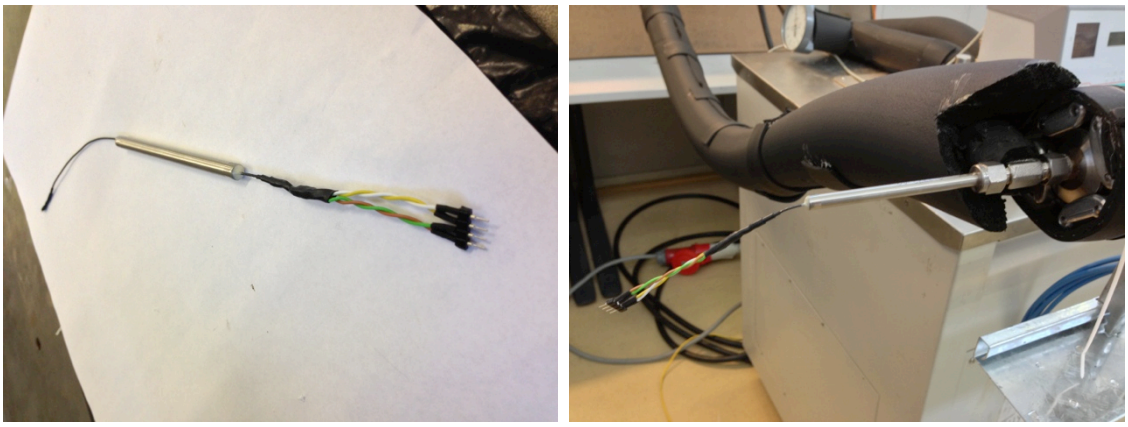
The accuracy is 0.1% of the output value.



Figure 6-3 Current source used for sensors' excitation.

6.1.3 Temperature sensors

For the purpose of the experiment PT100 sensors were used. Figure 6-4 presents sensor fabricated in such a way that it could float freely inside of the inner tube, supported by the Swagelok T-type connection. As a result a good contact between the measuring tip of the sensor and the coolant was achieved. This sensor was used to measure temperature of the coolant at the inlet of the transfer line.



a **b**

Figure 6-4 PT100 temperature sensor used at the inlet of the transfer line; a) sensor after manufacturing – tip of the sensor is in the top-left corner of the picture; b) sensor installed at the inlet of the transfer line;

Equation 6.1 was used to calculate temperature above 0°C.

$$T = -\frac{A}{2B} - \sqrt{\left(\frac{A}{2B}\right)^2 + \frac{\left(\frac{R}{100} - 1\right)}{B}} \qquad \text{Equation 6.1}$$

Where A,B are constants, R is resistance

Equation 6.2 was used to calculate temperature below 0°C.

$$T = A + BR + CR^2 + DR^3 + ER^4 + FR^5 \qquad \text{Equation 6.2}$$

Where A,B,C,D,E,F are constants, R is resistance

All the sensors were calibrated in a bath of C_6F_{14} before the measurements. Calibration was performed for the temperature range from -10°C to -45°C.

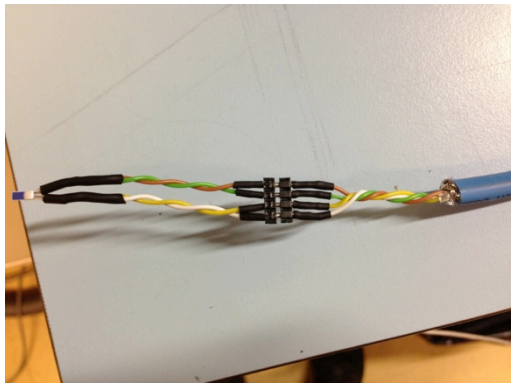


Figure 6-5 PT100 sensor used for the measurement of the surface and the ambient temperatures

Figure 6-5 presents a temperature sensor used for the surface and the ambient temperatures measurements. In total six sensors of that type were used. Equation 6.3 presents formula used to calculate the error of measurements above 0°C and Equation 6.4 presents the formula used for calculations below 0°C respectively.

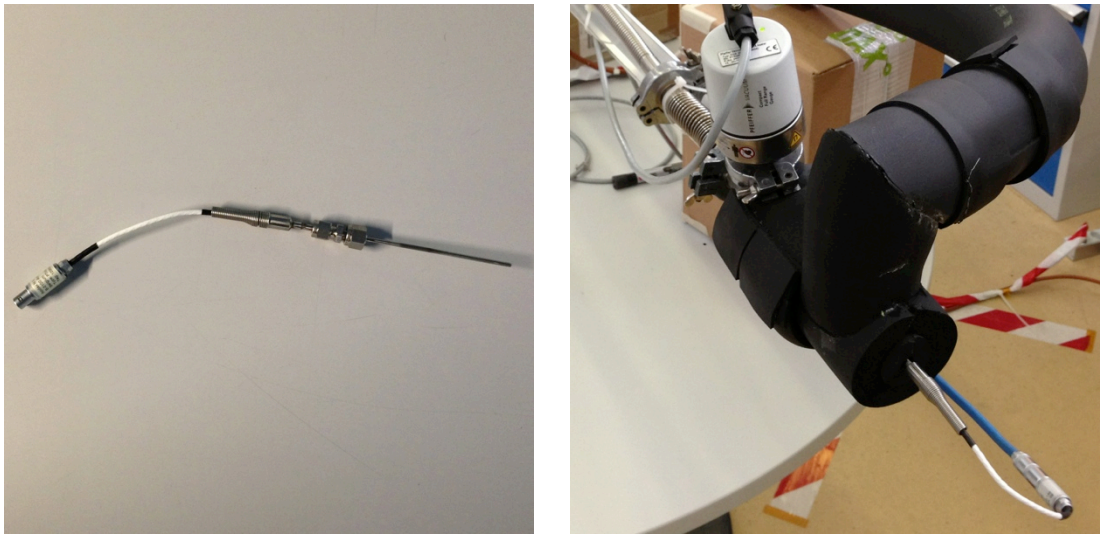
$$\Delta t = -0.002t + 0.15 \qquad \text{Equation 6.3}$$

Where t is temperature

$$\Delta t = 0.002t + 0.15 \qquad \text{Equation 6.4}$$

Where t is temperature

Figure 6-6 presents the temperature sensor used for the measurement of the coolant at the outlet of the transfer line. In this case a standard temperature sensor was used as the coolant remained in good contact with the measuring tip of the sensor.



a **b**

Figure 6-6 PT100 temperature sensor used to measure coolant temperature at the outlet of the transfer line; a) sensor after the measurement with Swagelok components on it; b) temperature inside of the transfer line

6.1.4 Mass flow meter

The measurements were performed for specific mass flow rates. A KROHNE mass flow meter using Coriolis mass flow measuring principle was used for this reason. Its accuracy was calculated based on the equation Equation 6.5. The mass flow rate of 6g/s was decided to be the reference value for which all of the measurements had to performed. Below that value the signal was getting too noisy and inconsistent. The maximum mass flow level achieved was in range between 9g/s and 10g/s.

Equation 6.5 presents the formula used to calculate the mass flow rate measurement error.

$$\Delta\dot{m} = 0{,}000002\dot{m}^6 - 0{,}00008\dot{m}^5 + 0{,}0013\dot{m}^4 - 0{,}0115\dot{m}^3 + 0{,}0594\dot{m}^2 - 0{,}1803\dot{m} + 0{,}3976 \qquad \text{Equation 6.5}$$

Where $\dot{m}$ is the mass flow rate

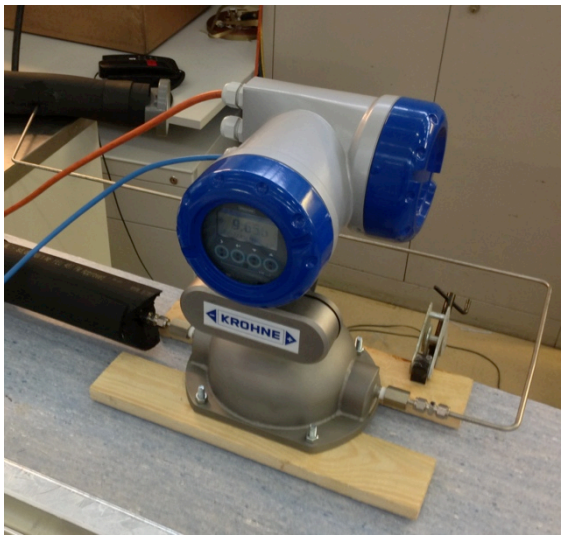


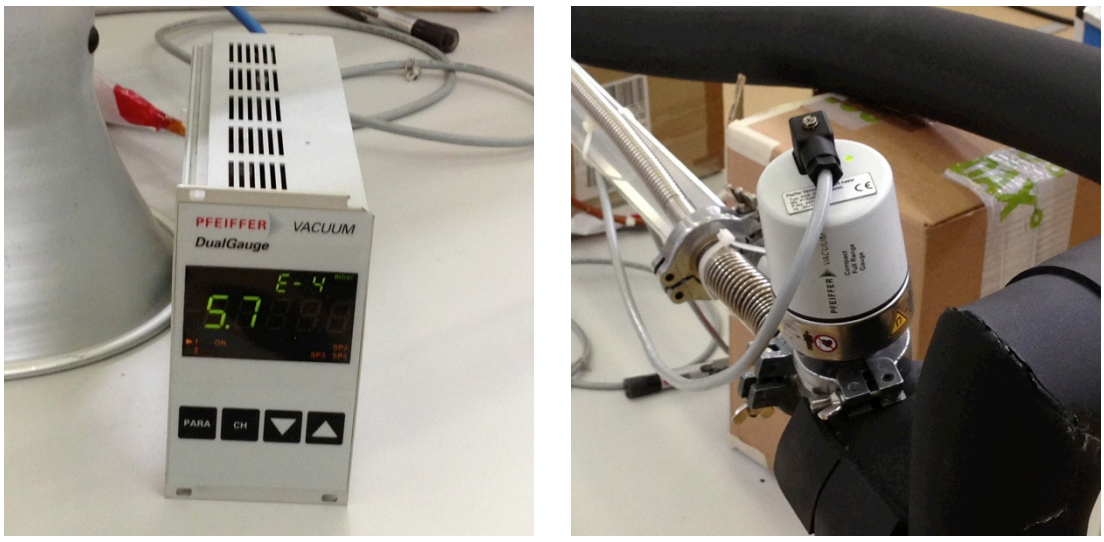
Figure 6-7 KROHNE mass flow meter

Figure 6-7 presents mass flow meter implemented at the end of the loop with the coolant. Needle valve used to control the mass flow rate was installed on the straight section of the return line.

6.1.5 Vacuum gauge

In order to measure the vacuum a vacuum gauge was installed next to the outlet of the transfer line. The vacuum pump was at the opposite end. Therefore, the indicated pressure was the worst pressure present in the insulated vacuum space of the transfer line.

The vacuum gauge was connected with its control unit that was connected to the multimeter. Its accuracy is ±30% in the range $1x10^{-8}$…100mbar.



a **b**

Figure 6-8 a) PFEIFFER Dual Gauge™ TPG 262 channel measurement and control unit for compact gauges; b) PFEIFFER Compact FullRange™ gauge;

6.1.6 LabVIEW program

All of the necessary conversions of the voltage signal from the multimeter to the temperatures, pressure or mass flow rate values were performed in LabVIEW environment. A special program was created to observe values of interest during the measurement and to save the data to a text file for a later analysis.

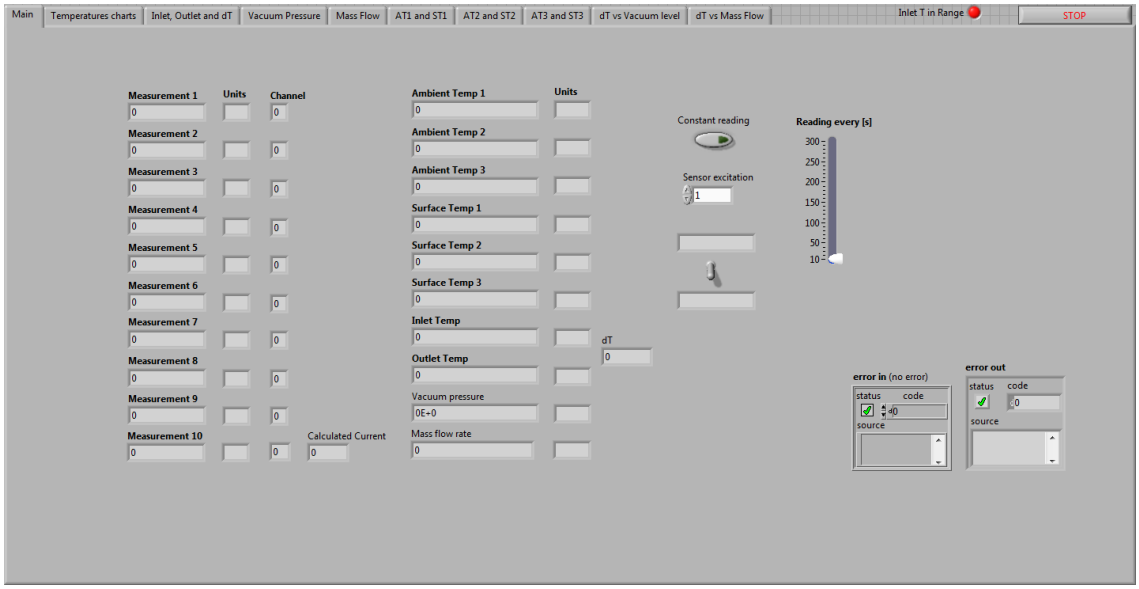


Figure 6-9 Main screen of the user interface in LabVIEW.

6.1.7 Measurement accuracy

In order to calculate the accuracy of the temperature measurements the Equation 6.6 was used to obtain the resistance error.

$$\frac{\Delta R}{R} = \frac{\Delta U}{U} + \frac{\Delta I}{I} \qquad \text{Equation 6.6}$$

Where R is resistance, U is voltage, I is current

The Direct Current Voltage characteristics are calculated from the Equation 6.7.

$$\Delta U = 40\text{ppm of reading} + 35\text{ppm of range} \qquad \text{Equation 6.7}$$

Where ppm is parts per million

Given resistance for PT100 sensors at -40°C equal to ≈ 84 Ω, excitation current equal to 1mA and resolution of the multimeter equal to 0.1 µV in 100 mV range:

$$\Delta U = 6.86\ \mu V \qquad \text{Equation 6.8}$$

As the temperatures sensors are excited with the same current during the calibration and the measurements Equation 6.6 becomes:

$$\frac{\Delta R}{R} = \frac{\Delta U}{U} \qquad \text{Equation 6.9}$$

Given Equation 6.8 and Equation 6.9

$$\Delta R = 6.9 * 10^{-3}\ \Omega \qquad \text{Equation 6.10}$$

Given sensitivity of the temperature sensor equal to 2.55 $\frac{K}{\Omega}$

$$\Delta T \approx 0.04\ K \qquad \text{Equation 6.11}$$

Equation 6.11 gives measurement accuracy for the temperature differences between the temperature of the coolant at the inlet and the outlet of the transfer line.

In the same manner was obtained accuracy for the temperature differences between the surface and ambient temperatures, which is presented in Equation 6.12.

$$\Delta T \approx 0.06\ K \qquad \text{Equation 6.12}$$

6.2 Peripheral devices

This subchapter aims at presenting auxiliary devices needed to control flow of the coolant in the experiment loop – chiller, or achieve and control vacuum pressure – vacuum pump. The bake-out process preceded in the measurements is described.

Additionally, the IR camera used to take the infrared pictures of the transfer line during the measurements is presented.

6.2.1 Chiller

The coolant used in this experiment was cooled down to the respective temperatures using the Julabo FPW 31 chiller, which is presented on Figure 6-11.

Study of the thermal performance of the transfer line was executed using C_6F_{14} refrigerant. The choice of the refrigerant was motivated by its boiling point being 56 °C at atmospheric pressure. This particular pressure is high enough to ensure that the flow in the experiment loop was at a liquid phase. Figure 6-10 presents saturation curve of C_6F_{14} with operation range during the experiment.

The temperature of the coolant was controlled by a control unit on the top of the chiller by setting the set point. In addition it was allowed to control the speed of the pump inside of the chiller. Endeavours were taken to keep the pump setting at its highest level in order to limit, when possible, the fluctuations in the mass flow rate.

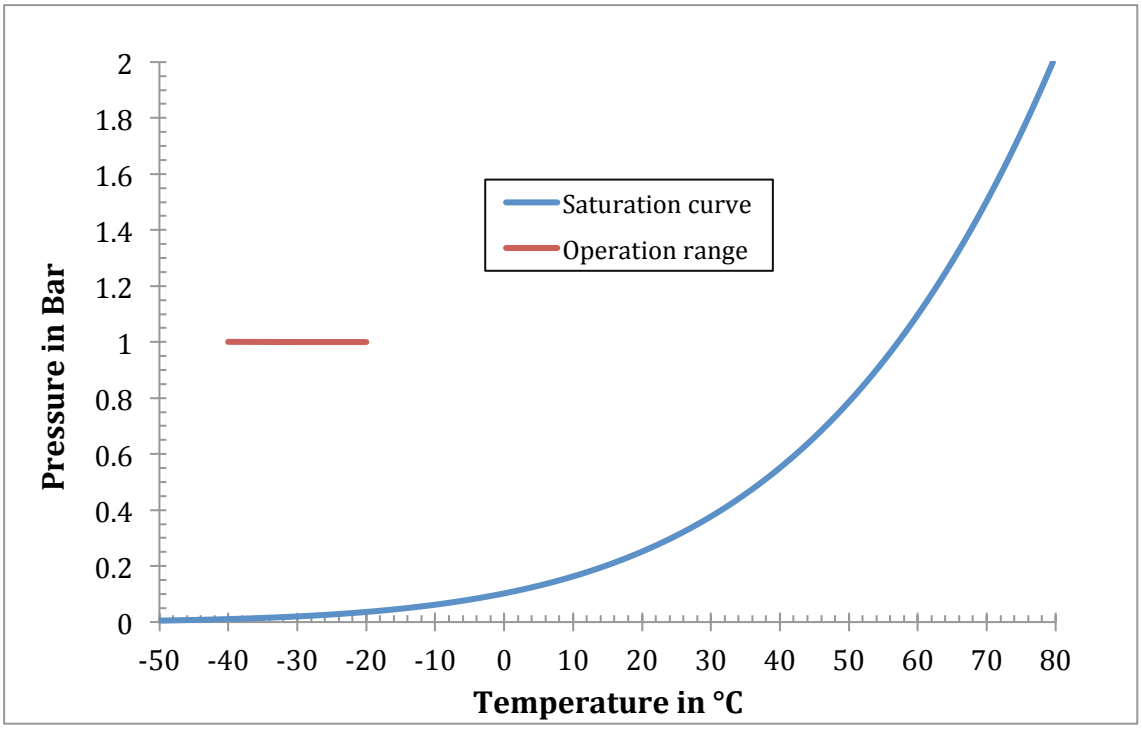


Figure 6-10 Pressure - temperature diagram of C_6F_{14} with saturation curve **[16]**.



Figure 6-11 Julabo FPW 31 chiller.

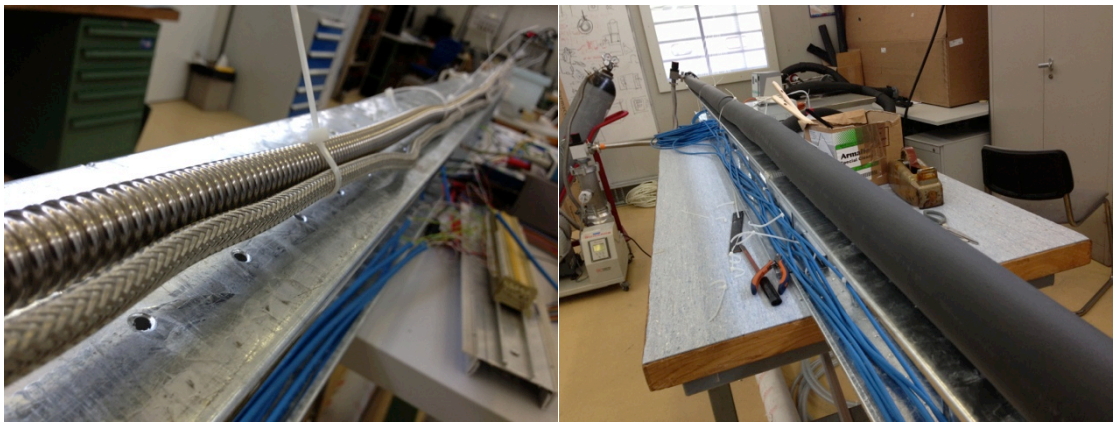
6.2.2 Vacuum pump

To create the necessary vacuum in the transfer line a pumping station consisting of a scroll and a turbomolecular pump was used. The pumping station is presented on Figure 6-12. All of the measurements were conducted at two vacuum levels that were achieved by switching on or off the turbomolecular pump.



Figure 6-12 EDWARDS Vacuum pump. On the left hand side can be seen the backing pump and on the right hand side the turbomolecular pump

Before the measurements took place the bake-out was performed in order to get rid of the moisture inside of the transfer line. The heating cable was attached besides the transfer line and insulated with Armaflex insulation resistant to high temperatures.



a **b**

Figure 6-13 Transfer line before the bake-out; a) heating cable attached to the transfer line; b) transfer line before the bake-out insulated with Armaflex;

6.2.3 IR camera

In order to observe temperature distribution on the surface of the transfer line the FLIR IR camera was used. Before the measurements transfer line was painted in black matte colour to increase emissivity.

Furthermore, a chimney made out of card-box was employed to minimize the amount of light entering the measurement areas. Furthermore all of the measurements were performed by night to minimize reflections. Despite of all the precautions taken, as explained in detail in Results Chapter 7, the data gathered was greatly influenced by external conditions.

Accuracy provided in the technical specification of the camera is ±2 °C for the range between -20°C and 120°C. Therefore, the measurement error is even greater, as most of the temperatures measured were below -20°C. However, it still provides a good overview of the temperature differences along the length of the transfer line.



Figure 6-14 FLIR IR camera used for taking pictures of the transfer line.

6.3 Measurement configurations

This subchapter aims at presenting all of the configurations in which the measurements were performed. The transfer line had to be checked for different scenarios, therefore, appropriate measuring setups had to be prepared.

Figure 6-15 presents a process flow diagram for the measurements in straight configuration. Aftet these measurements the transfer line was coiled, which is presented in Figure 6-21.

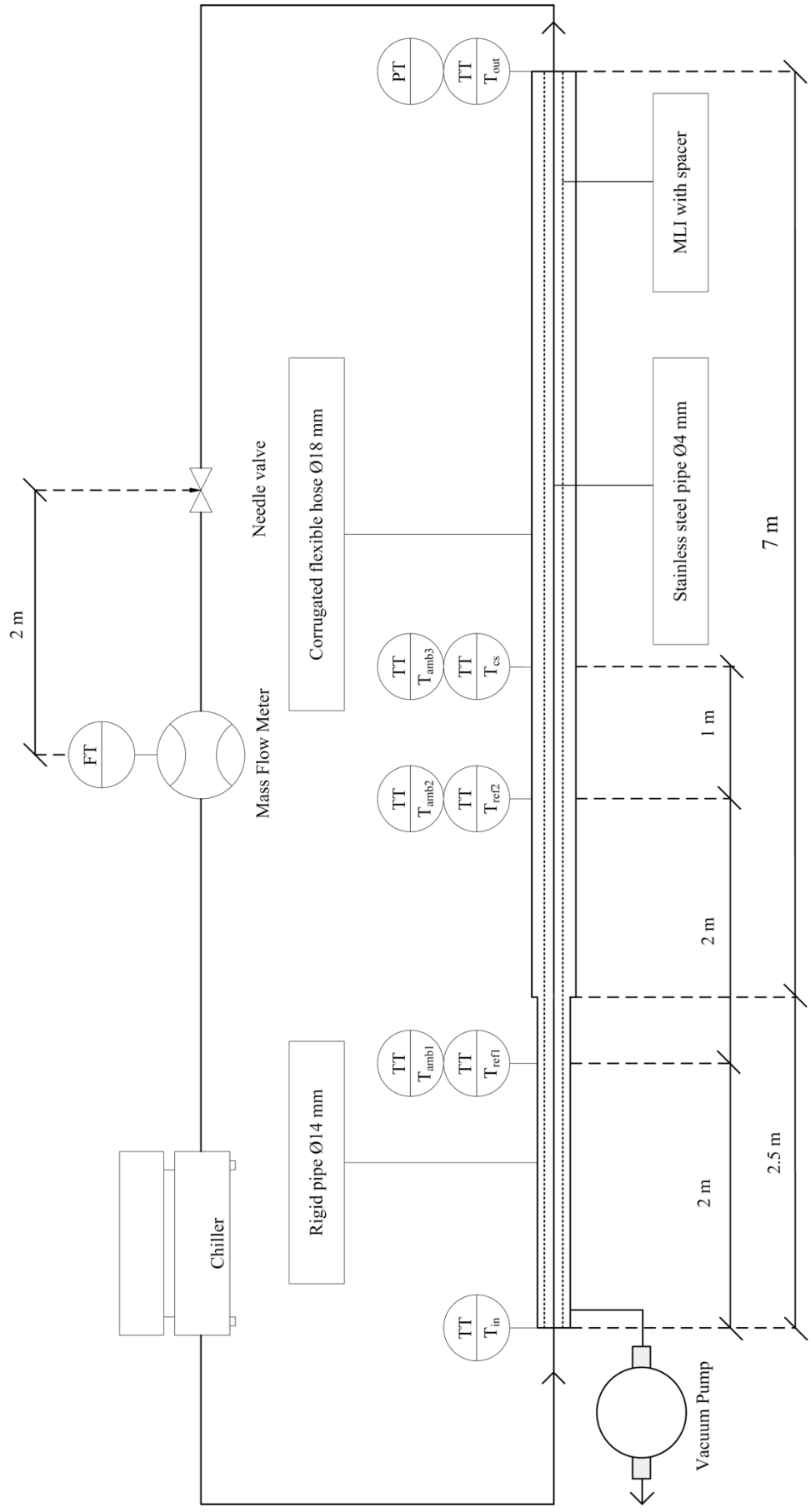


Figure 6-15 Process flow diagram of the experimental setup in straight configuration

6.3.1 Straight configuration

First series of measurements were performed in a straight configuration. The transfer line was stretched across the laboratory and no bending was applied to any part of it; so that, the basic performance of the transfer line could be defined. The measurements taken in this configuration were treated as the reference measurements; in other words as a best-case scenario.

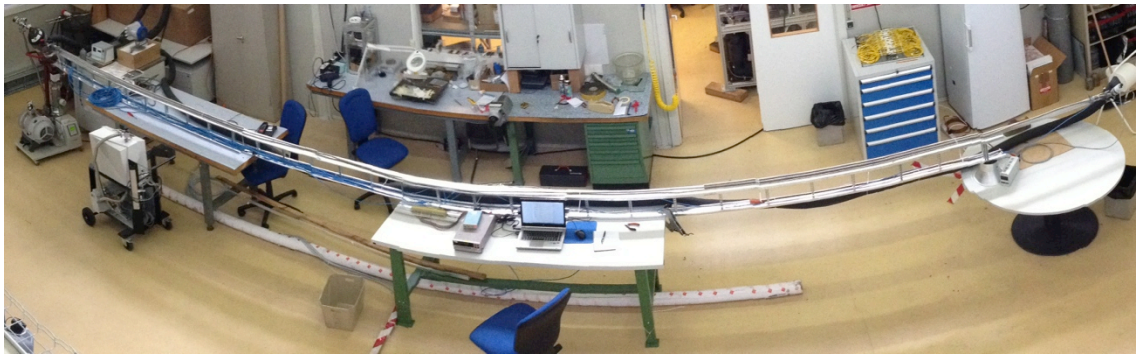


Figure 6-16 Panoramic view of the transfer line in straight configuration.



Figure 6-17 Transfer line in straight configuration with temperature sensors installed on it.

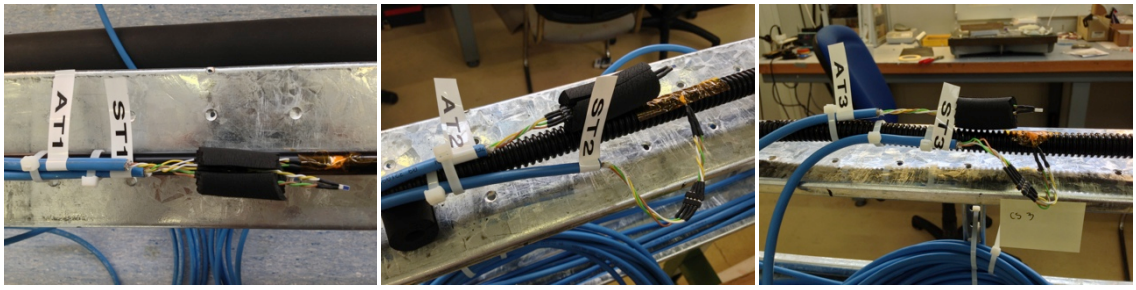
Figure 6-16 presents the transfer line in a straight configuration in the laboratory. The vacuum pump with chiller is situated on the left – inlet side. Vacuum gauge with control unit is on the right hand side next to the outlet of the transfer line. The desk in the middle holds DAQ components.

Figure 6-17 presents transfer line in a straight configuration with temperature sensors installed on it. The sensors are covered with plastic foil in order to reduce the fluctuations in temperature caused by air movements.

Particular temperature sensors are presented in Figure 6-18. In addition to the measurement of the temperature of the coolant at the inlet and the outlet of the transfer line, there were three pairs of temperature sensors used in this measurement installed on the transfer line.

Temperature sensors were situated on the transfer line after observing temperature distribution on its surface with the IR camera. Reference and cold spots were localized. Cold spots are areas on the surface of the transfer line with the highest temperature difference to the ambient temperature, whereas reference spots are those with the smallest. It is assumed that cold spots occurrence is caused by the minimized distance between the inner tube and the outer tube or flexible hose of the transfer line.

Two reference spots were chosen for the measurements with the temperature sensors. One spot on the rigid tube of the transfer line and one on the flexible hose. Additionally it was decided to measure one cold spot on the flexible part of the transfer line, which can be observed in Figure 6-18c.



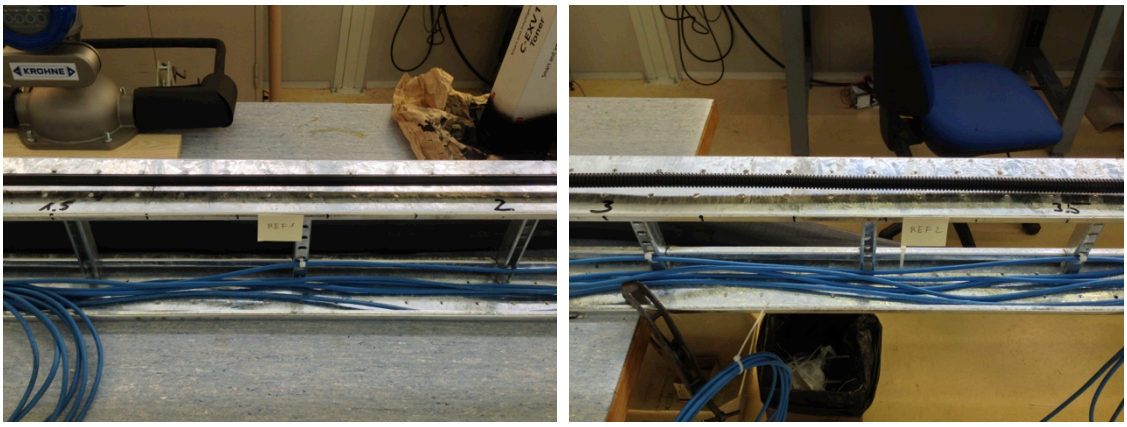
a **b** **c**

Figure 6-18 Temperature sensors installed on the transfer line used for the ambient and the surface temperature measurements; a) temperature sensors pair no. 1 installed on the reference point of the rigid part of the transfer line; b) temperature sensors pair no. 2 installed on the reference point of the flexible part of the transfer line; c) temperature sensors pair no. 3 installed on the cold spot on the flexible part of the transfer line;

For the IR camera measurements two reference points were found as well, which can be observed on Figure 6-19. Pictures were taken and images of two cold spots out of three can be observed on Figure 6-20.

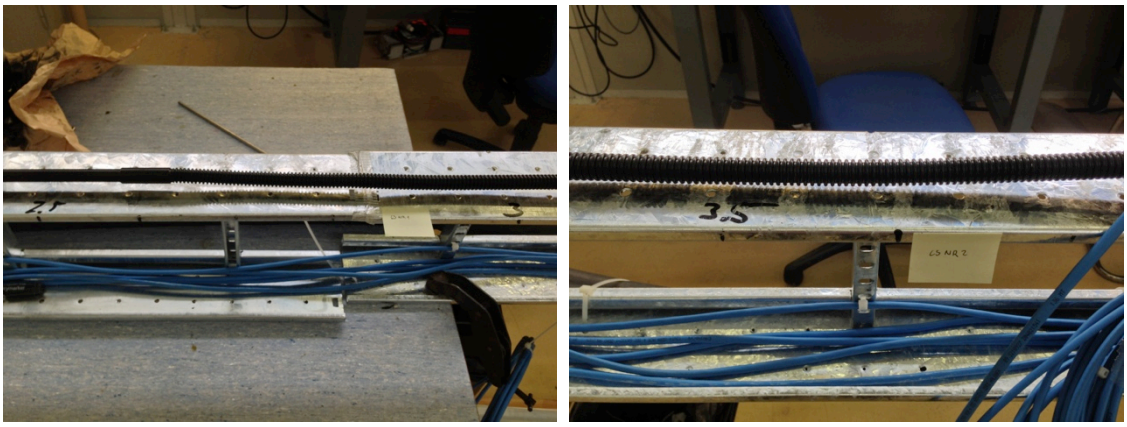
Black digits marked in Figure 6-19 and Figure 6-20 represent the distance in meters from the inlet of the transfer line.

The measured cold spots were the most severe ones that could be found, however, as explained in Chapter 7 it was relatively difficult to find any at all in this configuration of the transfer line.



a **b**

Figure 6-19 Spots where the IR pictures were taken; a) reference point 1 for IR pictures; b) reference point 2 for IR pictures;



a **b**

Figure 6-20 Spots where the IR pictures were taken; a) cold spot 1 observed with the IR camera; b) cold spot 2 observed with the IR camera

6.3.2 Coiled tight/relaxed configuration

The second set of measurements was taken in tight/relaxed configuration of the transfer line. This configuration was created by bending the transfer around a metal cylinder of 10 cm in diameter.

Firstly, the transfer line was bend around the cylinder with a great force and clumped. This setup corresponds to tight configuration. Secondly, the clamps were opened and the transfer line was relieved slightly so that the inner pipe of the transfer line did not exert that much stress on the outer hose of the transfer line. This case scenario corresponds to coiled – relaxed configuration.

In this configuration the temperature sensors were installed only on the flexible part of the transfer line, as the rigid part remained unmodified.

Again, in this scenario a cold spot and the reference point were found and measured with the temperature sensors and the IR camera.

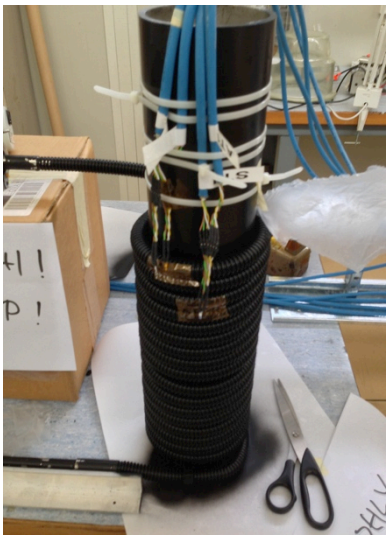
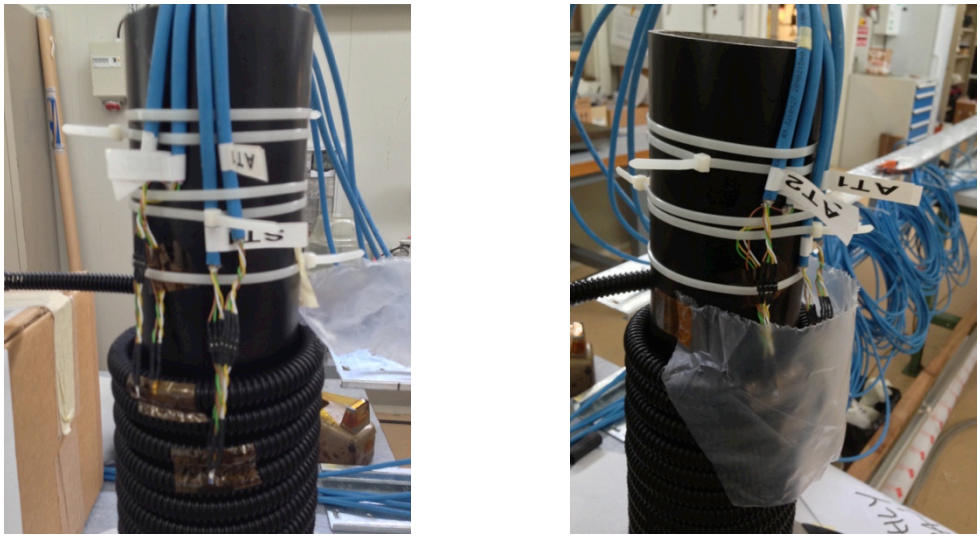


Figure 6-21 Transfer line in coiled – tight/relaxed configuration

Figure 6-21 presents the transfer line in coiled configuration with temperature sensors installed on the surface. Temperature sensors pair No.1 was installed on the reference point of the transfer line, whereas pair No.2 on the cold spot.

Based on Figure 6-22b it can be observed that a plastic foil was used again to reduce the fluctuations in measurements caused by air movements in the laboratory.



a **b**

Figure 6-22 Temperature sensors installed on the transfer line in coiled tight/relaxed configuration; a) Temperature sensors pair No. 1 installed on the reference point of the transfer line; b) temperature sensors pair No. 2 installed on the called spot of the transfer line

6.3.3 Bent rigid part of the transfer line

This measurement configuration was devoted to the observation of the performance of the transfer line with the rigid pipe bent at 90 degrees angle. The rest of the transfer line remained in coiled – relaxed configuration.

Based on the figure Figure 6-24 it can be observed that the temperature sensors of pair No. 2 were installed on the cold spot of the transfer line, which was found directly at the bend. The reference point sensors pair was situated around 20 cm next to the bend.

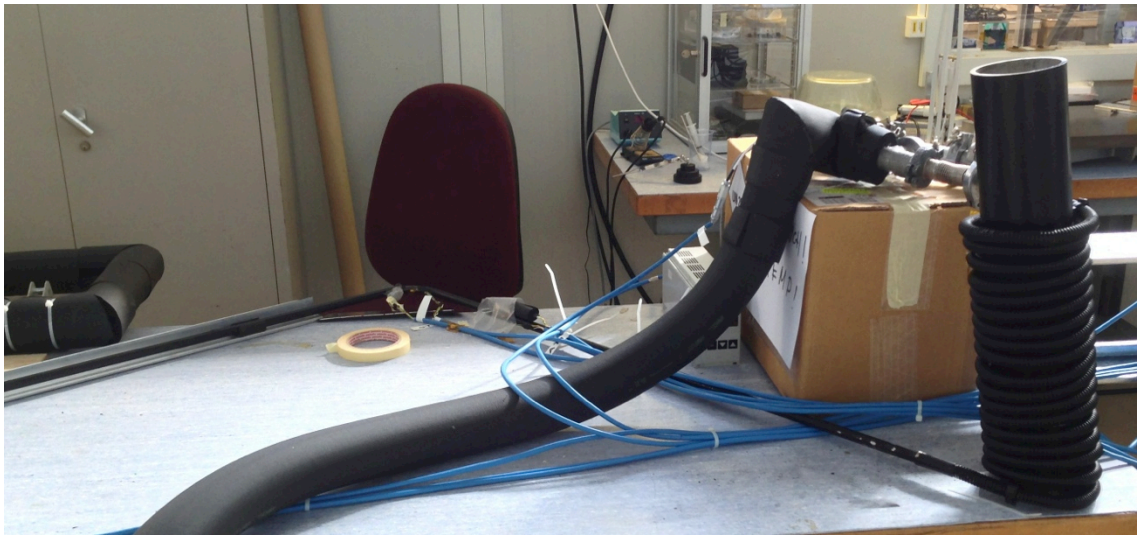


Figure 6-23 Transfer line after bending of the rigid part.

This measurement configuration represents worse than expected scenario, as in the ATLAS experiment cavern it is not planned to bend the transfer line to such a high degree.



Figure 6-24 Temperature sensors installed on the bent rigid part of the transfer line

7 Results

This chapter aims at presenting the results obtained during the experiment with the CO_2 flexible vacuum insulated transfer line. The majority of time at the beginning of the experiment was devoted to understanding the behaviour of the system and adapting all the necessary adjustments.

It was observed that ambient conditions had a great impact on the results. Therefore, all of the measurements were performed during the night in order to minimize the magnitude of the impact. Nevertheless, as it will be presented in the following parts of this chapter, often the measurement accuracy was not high enough to entirely eliminate the misleading impact of the environment.

The infrared (IR) pictures which were taken throughout the measurement provide an overview of the transfer lines, whereas the particular figures represent the accurate values.

Three different sets of measurements in straight configuration of the transfer line were performed. The experiment was started using that particular setup and the results led to the decision that it is sufficient to perform one set of measurements for every other configuration of the transfer line.

The common measurement for all of the configurations is at different vacuum levels. In cases when a good vacuum level was achieved, backing vacuum pump and turbomolecular pump were used at the same time. In cases of a worse vacuum level, only the backing vacuum pump was used. This choice of the vacuum pressures for the measurement was motivated by the fact that in case of turbomolecular pump failure the performance of the transfer line will be known to a certain degree of accuracy, which may facilitate the decision process in case of emergency.

7.1 Straight configuration

As pointed out in the introduction to this chapter, the measurements in a straight configuration were the first ones to be performed during the experiment. They provided the first insight into the transfer line performance and constituted the basis for the decision on how to proceed with the rest of the tests.

This section 7.1 is divided into three subsections. Each of the subsections firstly presents the temperature difference between the temperature of the coolant measured at the outlet and the inlet of the transfer line depending on either the mass flow rate, the temperature of the coolant measured at the inlet or the vacuum pressure. This helps the reader to understand the general performance of the transfer line and gives an overview on the expected temperature ranges.

Secondly, the subsections present the heat transfer as a function of the same varying features of the system, where applicable appropriate relations are concluded.

Lastly, the surface temperatures are studied. The temperature differences are depicted between the ambient temperatures and the surface temperatures, which are used to estimate the risk of condensation on the outer hose of the transfer line. Additionally, infrared pictures of the surface of the transfer line are presented in tables. Firstly, they were used for localization of the coldest spots on the outer hose of the transfer line, which led to sensors location. Secondly, they were

compared with the results obtained through the data acquisition system for the purposes of double-checking the measurements.

7.1.1 Measurements with different mass flow rates

This subsection presents the results obtained for three different mass flow rates of the refrigerant, while other parameters were kept constant. Measurements started with a mass flow rate of 6 g/s and finished with 9.4 g/s. The temperature of the refrigerant at the inlet was -40°C. The vacuum pressure was kept constant at the level of 1.9×10^{-4} mbar.

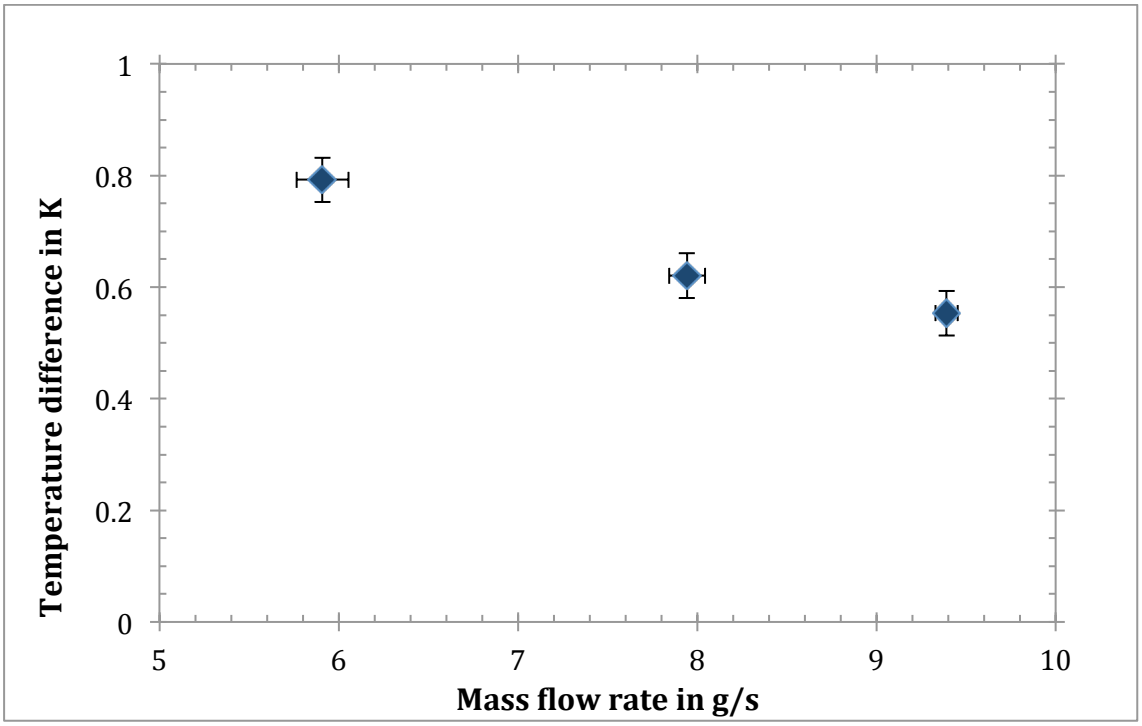


Figure 7-1 Temperature difference between inlet and outlet of the transfer line depending on the mass flow rate in straight configuration with temperature of the coolant measured at the inlet = -40°C.

On the Figure 7-1 it can be observed that the temperature difference of the coolant between outlet and the inlet of the transfer line does not exceed one Kelvin. This very first result shows clearly that vacuum acts as a good insulator and prevents an excessive heat transfer with the environment. Moreover, the figure depicts the fact that the higher the mass flow rate, the lower the temperature difference is. It is a result of the fact that the heat transfer remained constant for all the measurements. This can be observed on Figure 7-2.

Figure 7-3 yields results obtained during the measurement of the surface temperatures of the transfer line and ambient temperature. The temperature difference values are in the range from 0.28 K ± 0.38 K to 0.47 K ± 0.11 K. In this transfer line configuration the inner pipe with the coolant did not exert much force on the outer hose therefore the temperature difference for the cold spot remains roughly at same level as for the reference points.

Only by the analysis of the Table 7.1 with IR pictures it may be assumed that at the cold spots the inner pipe remained in contact with the outer hose or the distance between it and the outer hose was reduced comparing to the remaining part of the transfer line.

Due to the changing environmental conditions in the laboratory it is not possible to reason any further relations between the measurements by solely analysing the infrared pictures.

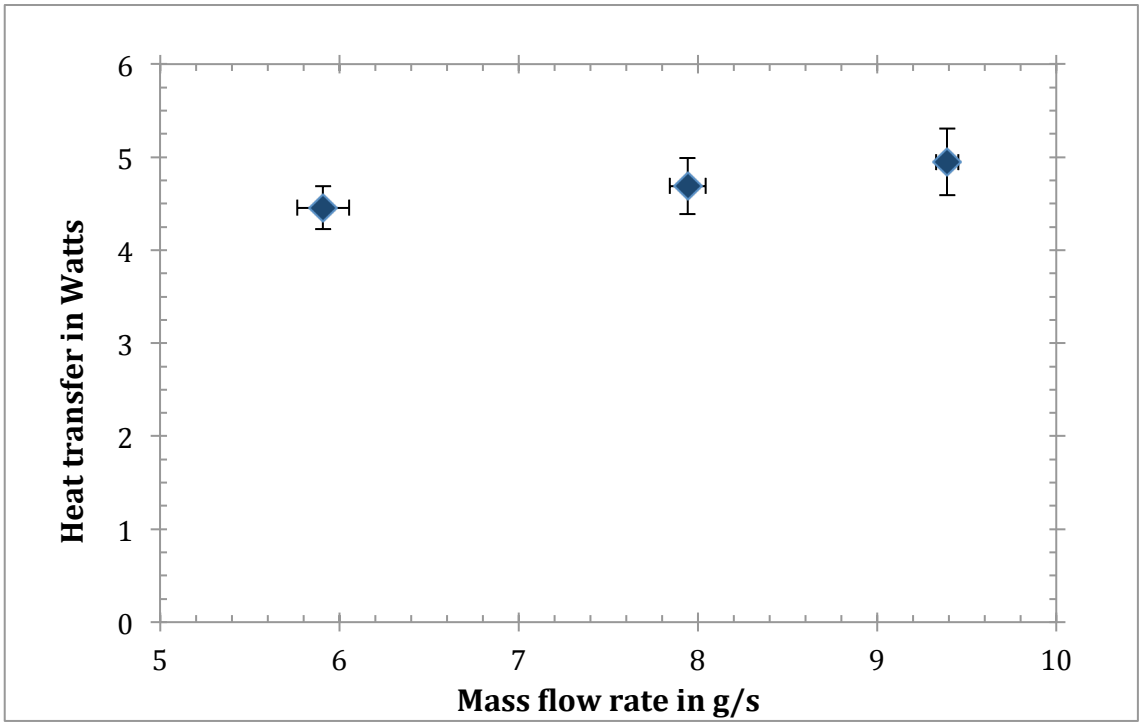


Figure 7-2 Heat transfer depending on mass flow rate during the measurement in straight configuration of the transfer line with the coolant temperature measured at the inlet = -40°C.

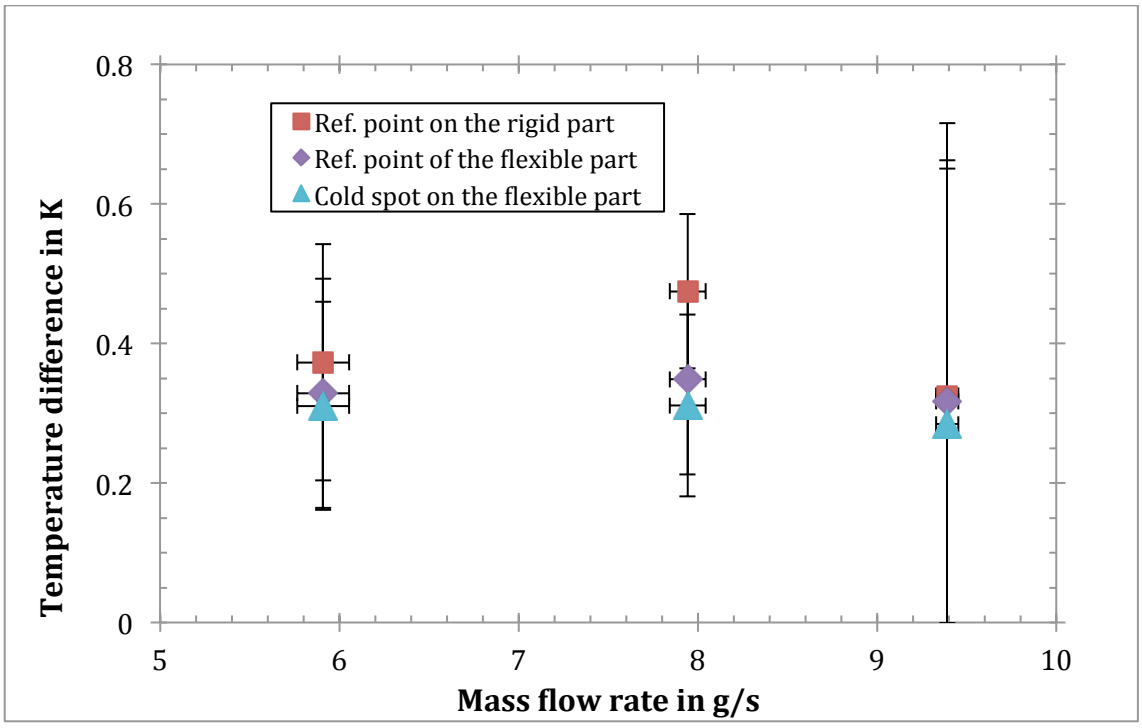
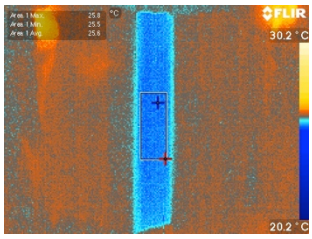
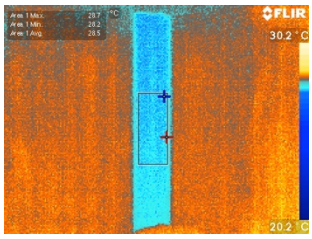
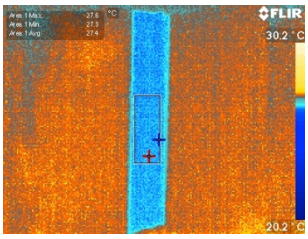
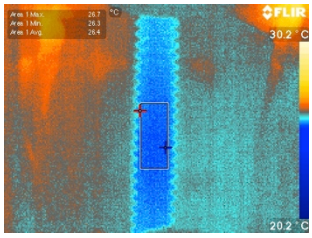
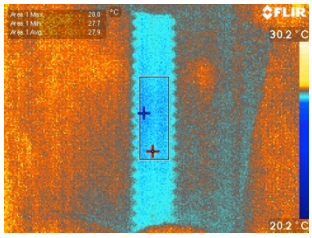
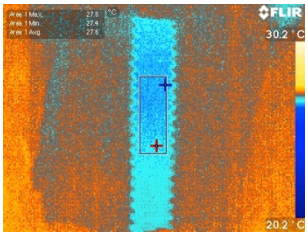
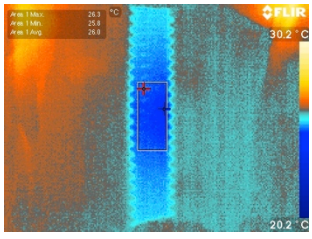
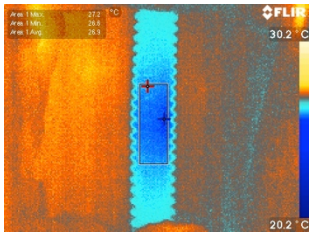
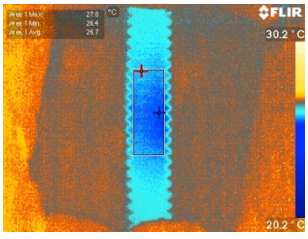
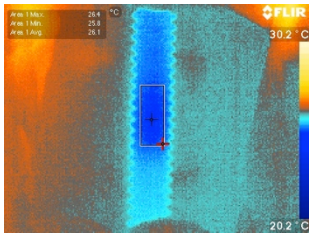
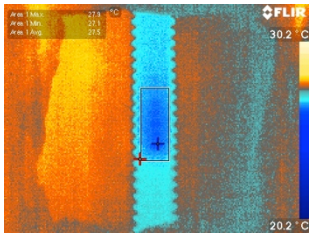
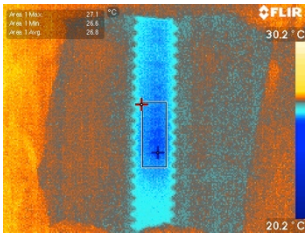
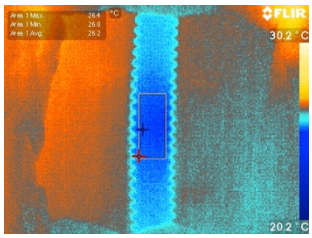
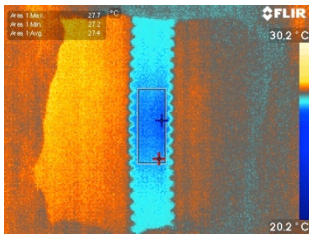
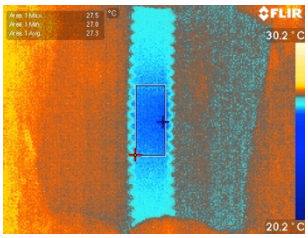


Figure 7-3 Temperature difference between ambient and surface temperature measured on the rigid and flexible part of the transfer line in straight configuration with different mass flow rates with the coolant temperature measured at the inlet = -40°C.

Table 7.1: IR pictures taken on five different spots of the transfer line for three different mass flow rates with the coolant temperature measured at the inlet = -40°C.

Mass flow rate	9.4 [g/s]	7.9 [g/s]	5.9 [g/s]
Reference Point 1	 t_{avg}= 25.6°C	 t_{avg}= 27.7°C	 t_{avg}= 26.7°C
Reference Point 2	 t_{avg}= 25.6°C	 t_{avg}= 27.1°C	 t_{avg}= 26.8°C
Cold Spot 1	 t_{avg}= 25.2°C	 t_{avg}= 26.1°C	 t_{avg}= 25.9°C
Cold Spot 2	 t_{avg}= 25.3°C	 t_{avg}= 26.7°C	 t_{avg}= 26°C
Cold Spot 4	 t_{avg}= 25.4°C	 t_{avg}= 26.6°C	 t_{avg}= 26.5°C

As envisaged on the above table, the IR pictures do not present any relation based on the mass flow rate. The only analogy can be found by comparing the reference points with the cold spots, which temperature is slightly lower.

7.1.2 Measurements at different coolant temperatures

Measurements at different coolant temperatures were performed by changing the set point on the Julabo chiller. These tests were made for three different settings of the chiller. The vacuum quality was kept as high as possible by using the turbomolecular pump. The mass flow rate was 6g/s.

Figure 7-4 depicts temperature differences of the coolant between inlet and outlet of the transfer line. It can be observed how it decreases as the coolant temperature rises. The obtained results are in accordance with the expectations. It is further confirmed by the Figure 7-5 which presents how the heat transfer decreased with the higher coolant temperature. In particular, the temperature difference between the temperature measured on the cold spot and the ambient temperature decreases greatly. This is caused by the reduced heat transfer by conduction. Temperatures differences between the reference points and ambient temperatures decrease at slower pace, as conduction in this case does not contribute as much as at the cold spots.

The same phenomenon is observed in the Figure 7-6 which shows temperature differences between ambient and surface temperatures depending on the coolant temperature. The temperature differences decrease while the coolant temperature increases. The differential between particular data point is small which is caused by a good performance of the transfer line at -40 °C.

At -20°C the temperature difference between ambient and surface temperature is getting closer to 0.1 K. This constitutes a further proof of good insulation properties of the used materials and the vacuum in the straight configuration of the transfer line.

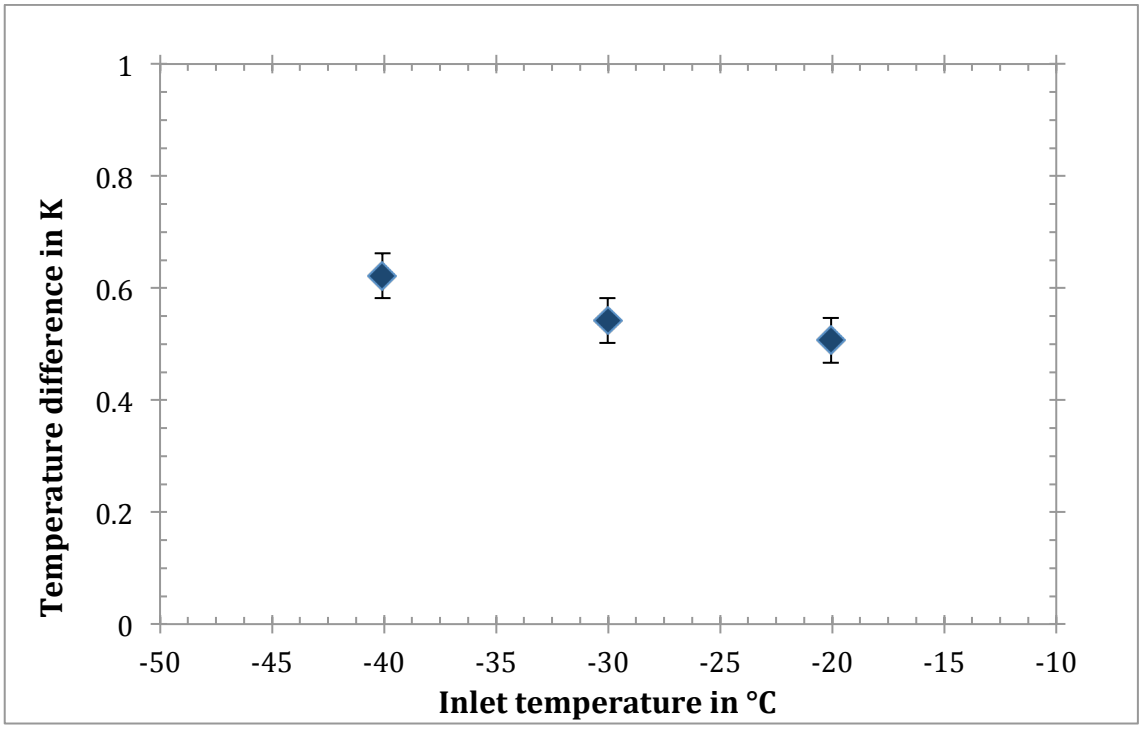


Figure 7-4 Temperature difference between inlet and outlet depending on the temperature of the coolant at the inlet with mass flow rate = 6 g/s.

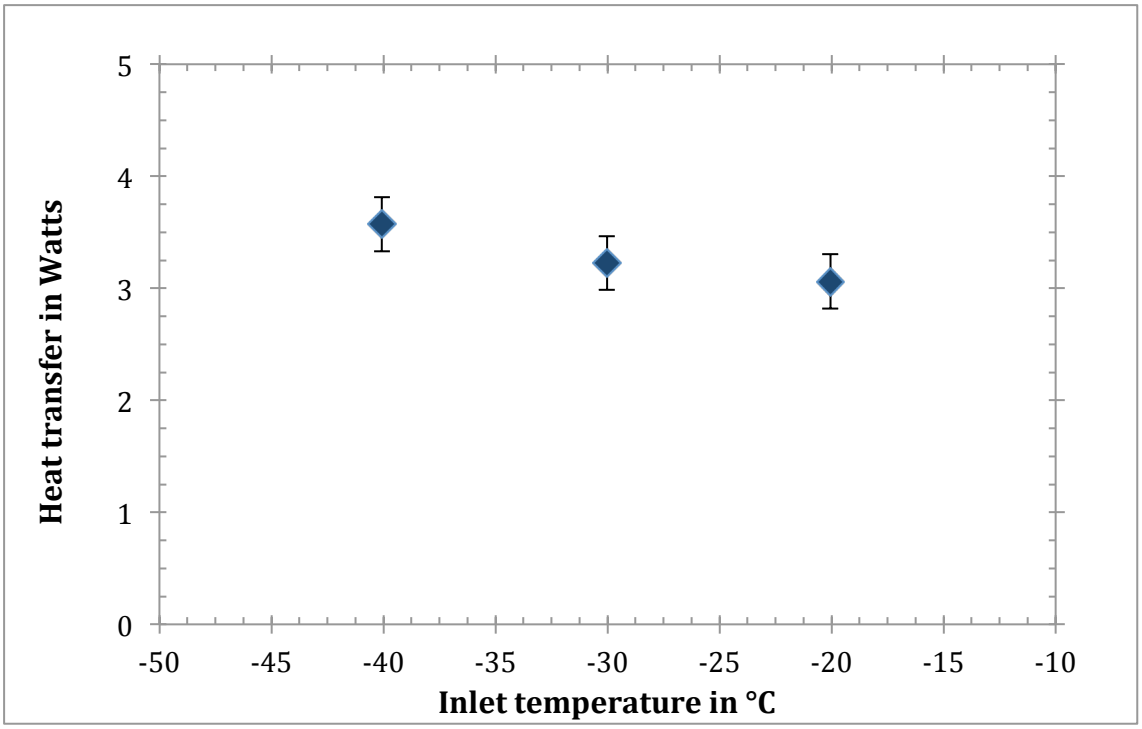


Figure 7-5 Heat transfer depending on the coolant temperature at the inlet of the transfer line during the measurement in straight configuration with mass flow rate = 6 g/s.

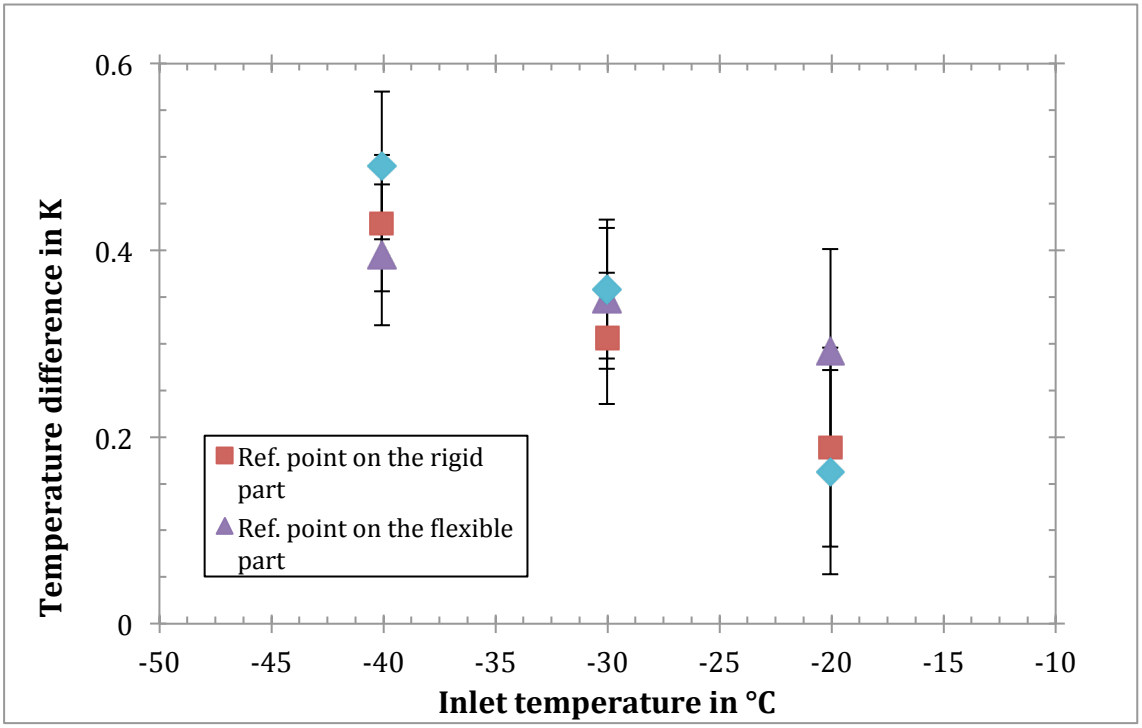


Figure 7-6 Temperature difference between ambient and surface temperatures measured on the rigid and flexible part of the transfer line in straight configuration with different coolant temperatures at the inlet with mass flow rate = 6 g/s.

Table 7.2: IR pictures taken on four different spots of the transfer line with different temperature of the coolant with mass flow rate = 6 g/s.

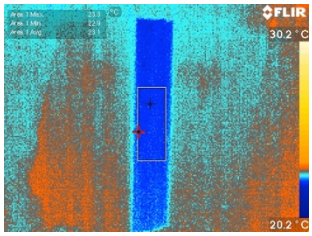
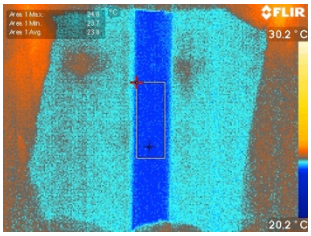
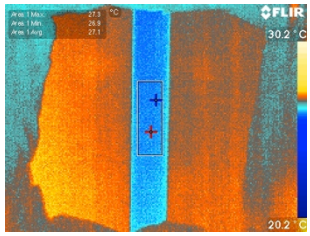
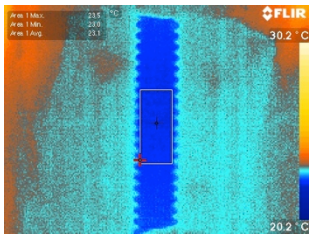
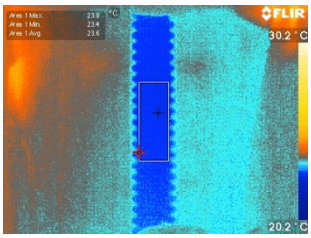
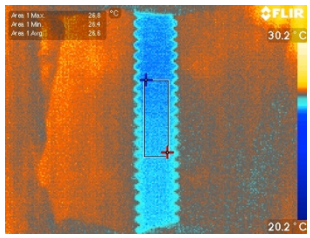
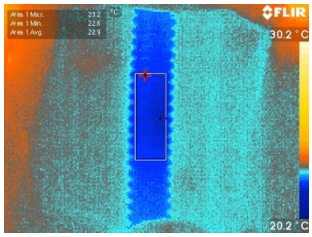
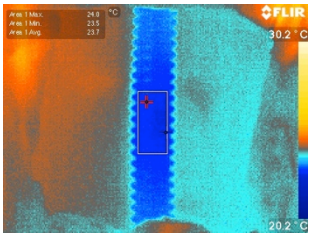
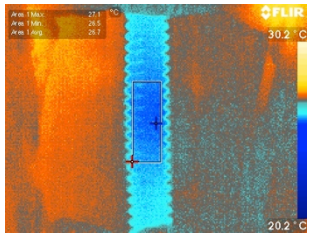
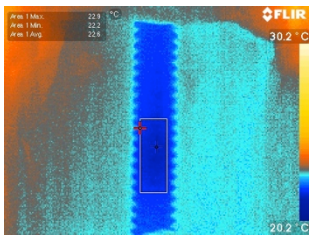
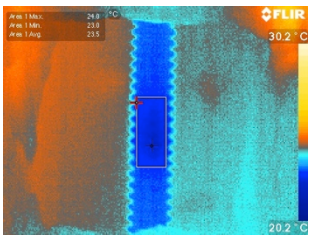
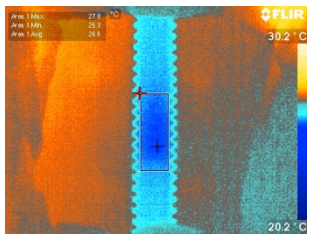
Coolant temp. at the inlet	-40 [°C]	-30 [°C]	-20 [°C]
Reference Point 1	 t_{avg}= 22.3°C	 t_{avg}= 23.0°C	 t_{avg}= 26.3°C
Reference Point 2	 t_{avg}= 22.3°C	 t_{avg}= 22.8°C	 t_{avg}= 26.6°C
Cold Spot 1	 t_{avg}= 22.1°C	 t_{avg}= 22.9°C	 t_{avg}= 25.9°C
Cold Spot 2	 t_{avg}= 21.7°C	 t_{avg}= 22.7°C	 t_{avg}= 25.9°C

Table 7.2 presents IR pictures of the transfer line taken during the measurements with different temperatures of the coolant. It can be clearly observed that the surface temperature of the transfer line increases along with the coolant temperature. The final differential between measurements at -40 °C and -20 °C is around 4 K, with the biggest difference observed between -30 °C and -20 °C. The obtained pictures are in accordance with the expectations, however, it needs to be kept in mind that the shown values were very prone to ambient conditions. Therefore, one has to use the results obtained with the data acquisition system and the IR pictures only for the reference purposes.

In this case apart of the Cold Spot 1 at -30 °C all of the cold spots have temperature slightly lower than the reference points. It confirms the fact that the greater proximity of the inner line has been localized appropriately. Nevertheless, the differences are still very low.

7.1.3 Measurements at different vacuum pressures

Last measurements in the straight configuration were performed at different vacuum levels. The mass flow rate was kept constant at 6 g/s and the temperature of the coolant measured at the inlet was -40 °C.

Based on the Figure 7-7 it may be observed that the temperature difference between the inlet and the outlet of the transfer line has increased slightly at worse vacuum level. However, the difference remains below one Kevin. As a result it may be stated that the transfer line can easily operate without significant loss of performance only with a backing pump. In case of a failure of the turbomolecular pump no special actions are required to prevent the coolant from condensation on the outer hose of the transfer line.

Figure 7-8 depicts heat transfer values during the measurement in straight configuration depending on the vacuum pressure. As expected by studying the temperature differences between the inlet and outlet of the transfer line the heat transfer has increased at worse vacuum level. Nevertheless, it is not of a high significance with respect to the performance of the transfer line.

Temperature differences between ambient and surface temperature of the transfer line are depicted in Figure 7-9. It can be deducted that the surface temperature has decreased at the worse vacuum level. However, once again the magnitude of change does not show anything that one, who would like to operate the transfer line in a straight configuration at this vacuum pressure, should be concerned about.

Figure 7-9 shows that the temperature measured at the cold spots is lower than reference points. However, the error bars do not allow stating this without any doubt. Therefore, once again the temperature distribution on the whole length of the transfer line turned out to be almost uniform.

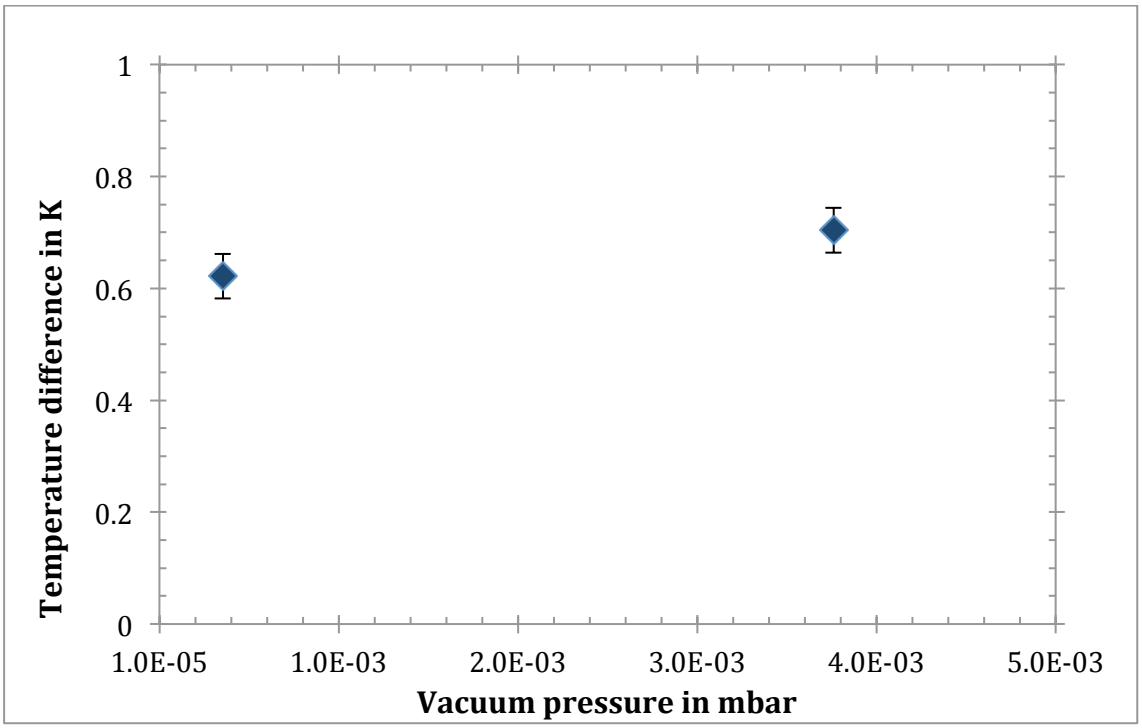


Figure 7-7 Temperature difference between inlet and outlet depending on vacuum pressure during the measurement in straight configuration with the coolant temperature measured at the inlet = -40°C.

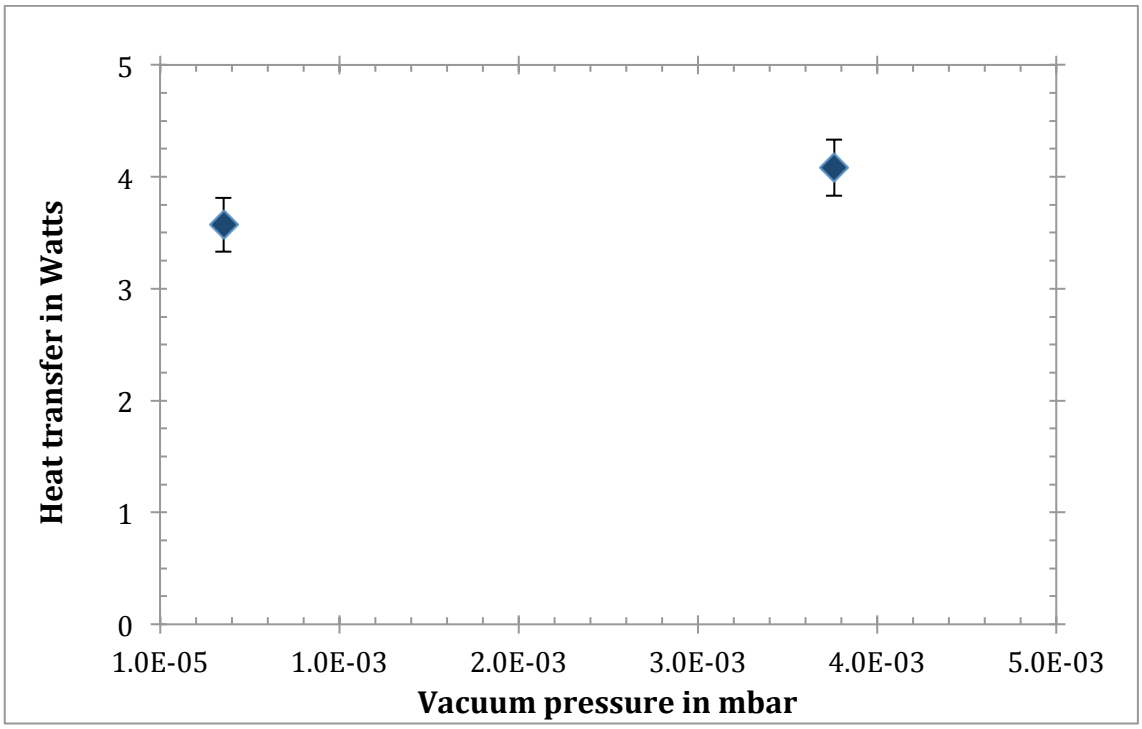


Figure 7-8 Heat transfer depending on vacuum pressure during the measurement in straight configuration with the coolant temperature measured at the inlet = -40°C.

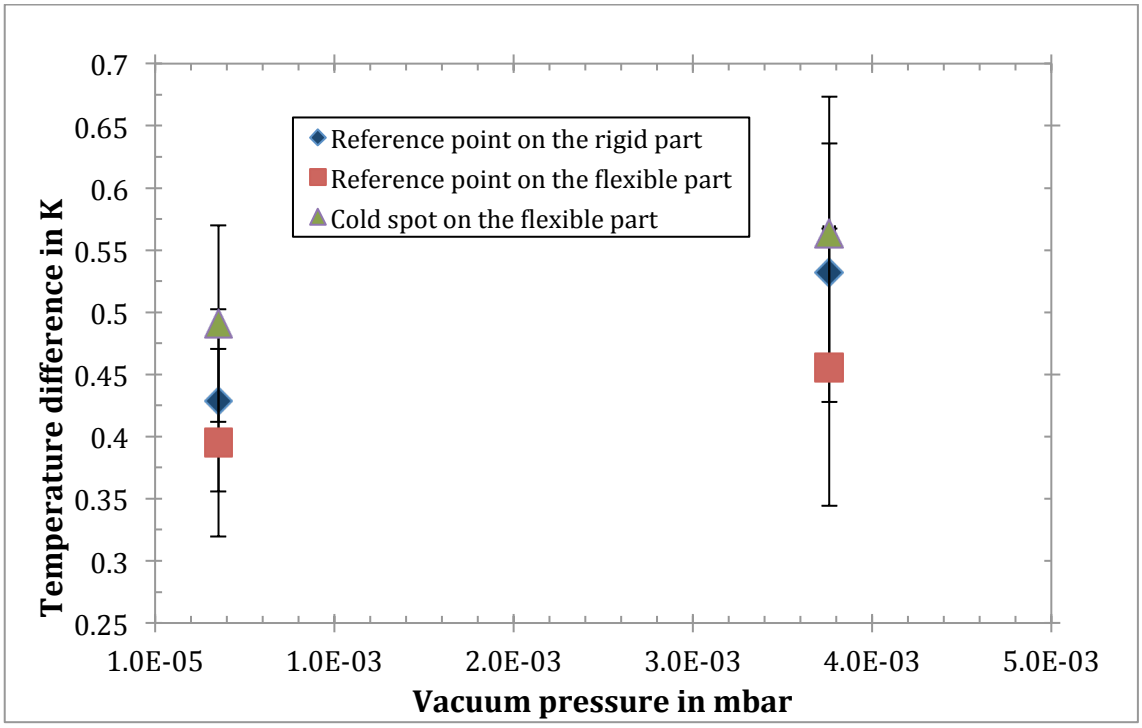


Figure 7-9 Difference between ambient and surface temperature measured on the rigid and flexible part of the transfer line in straight configuration at different vacuum pressures with the coolant temperature measured at the inlet = -40°C.

Table 7.3: IR pictures taken on four different spots of the transfer line during the measurements in straight configuration at different vacuum pressures with the coolant temperature measured at the inlet = -40°C and mass flow rate = 6g/s.

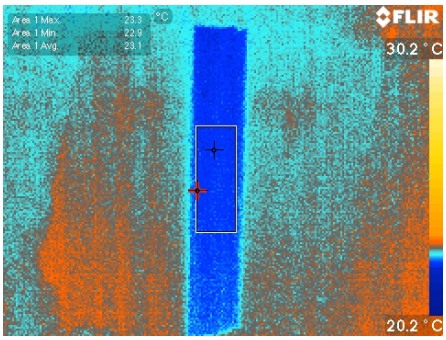
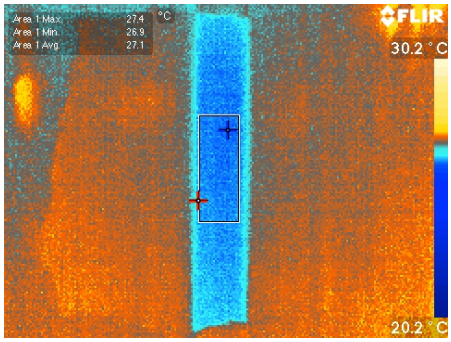
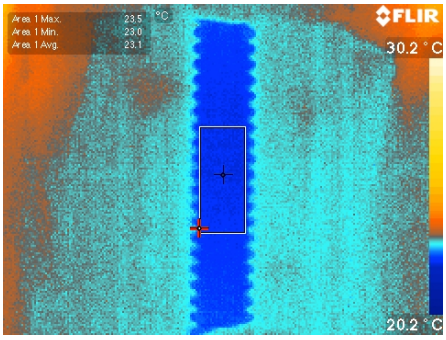
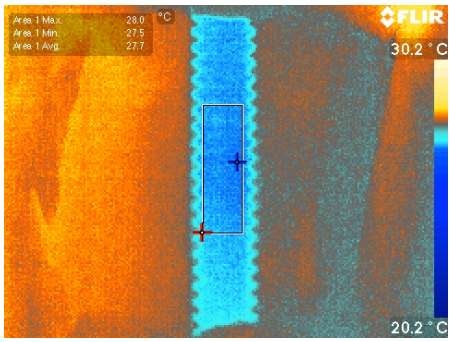
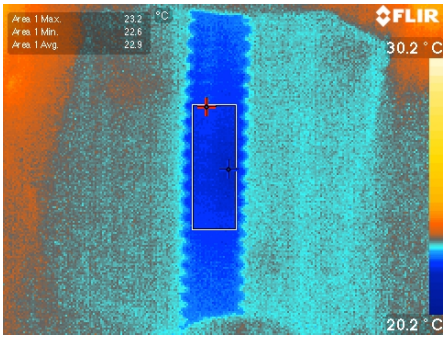
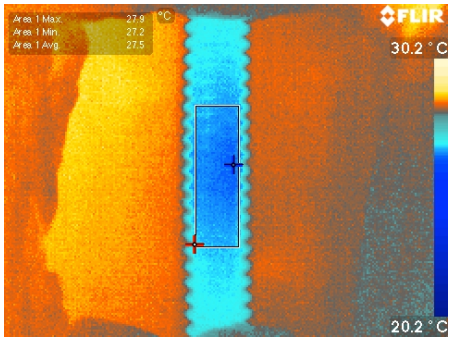
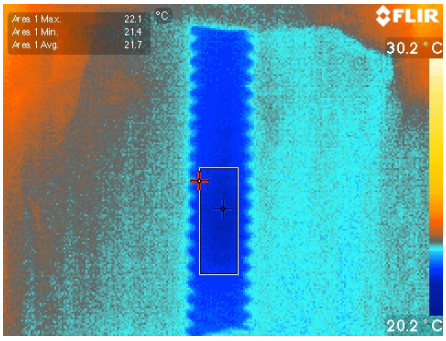
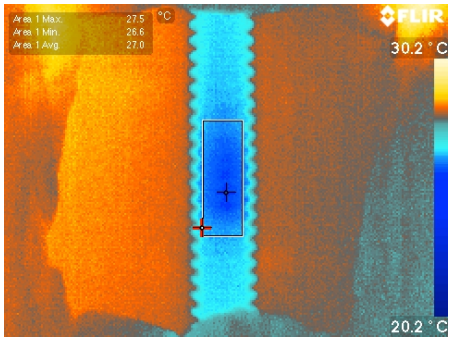
Vacuum pressure	3.5×10^{-4} [mbar]	3×10^{-3} [mbar]
Reference Point 1	 t_{avg}= 22.3°C	 t_{avg}= 26.4 °C
Reference Point 2	 t_{avg}= 22.3°C	 t_{avg}= 27.0°C
Cold Spot 1	 t_{avg}= 22.1°C	 t_{avg}= 26.7°C
Cold Spot 2	 t_{avg}= 21.7°C	 t_{avg}= 26.3°C

Table 7.3 represents four different spots of the transfer line at different vacuum pressures. The ambient condition influence was greater than the measurement accuracy, which prevents from drawing any conclusions. The only facts that can be clearly observed are the locations of the cold spots. However, their temperature is not much different from the reference points, therefore their impact will be neglected.

7.2 Coiled tight/relaxed configuration

The second set of measurements of the transfer line was performed in the coiled configuration of the transfer line. This section presents results which were obtained while the transfer line was kept tight around the cylinder and relaxed. As a consequence the magnitude of the influence of the inner pipe internal stress on the outer hose on the transfer line overall performance may be observed.

Measurements in this configuration were performed only at different vacuum pressures. This was a consequence of the fact that the previous measurements in a straight configuration have presented no significant dependencies of the mass flow rate or the temperature of the coolant on the performance of the transfer line in the measured range.

Figure 7-10 depicts temperature differences between the outlet and inlet of the transfer line depending on the vacuum pressure. In comparison to the measurements in a straight configuration now the differences exceed 1K. Even though some data points show almost double increase in temperature differences it is still not a very significant change if compared to other insulation technologies.

The temperature differences at different vacuum pressures in coiled – tight configuration remained at the same level, whereas for coiled – relaxed configuration has slightly increased. This once again proves the fact that the transfer line can operate well within this vacuum pressure range.

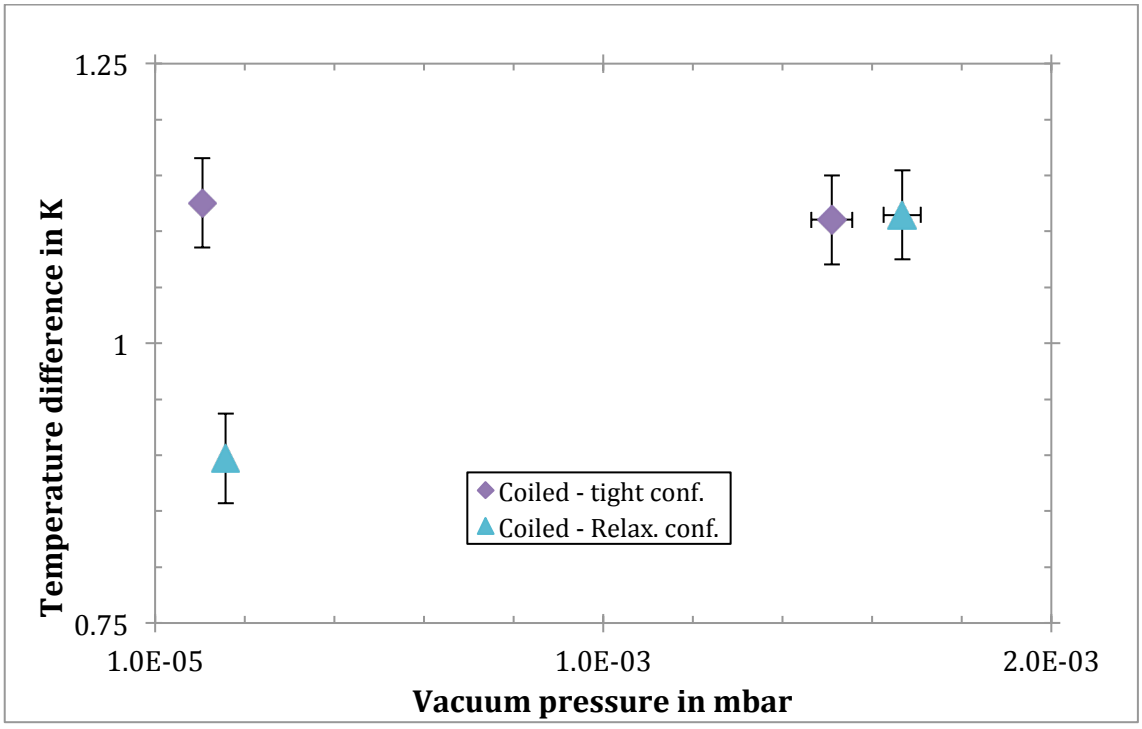


Figure 7-10 Temperature difference between outlet and inlet temperature measured in coiled - tight and coiled - relaxed configuration of the transfer line at different vacuum pressures.

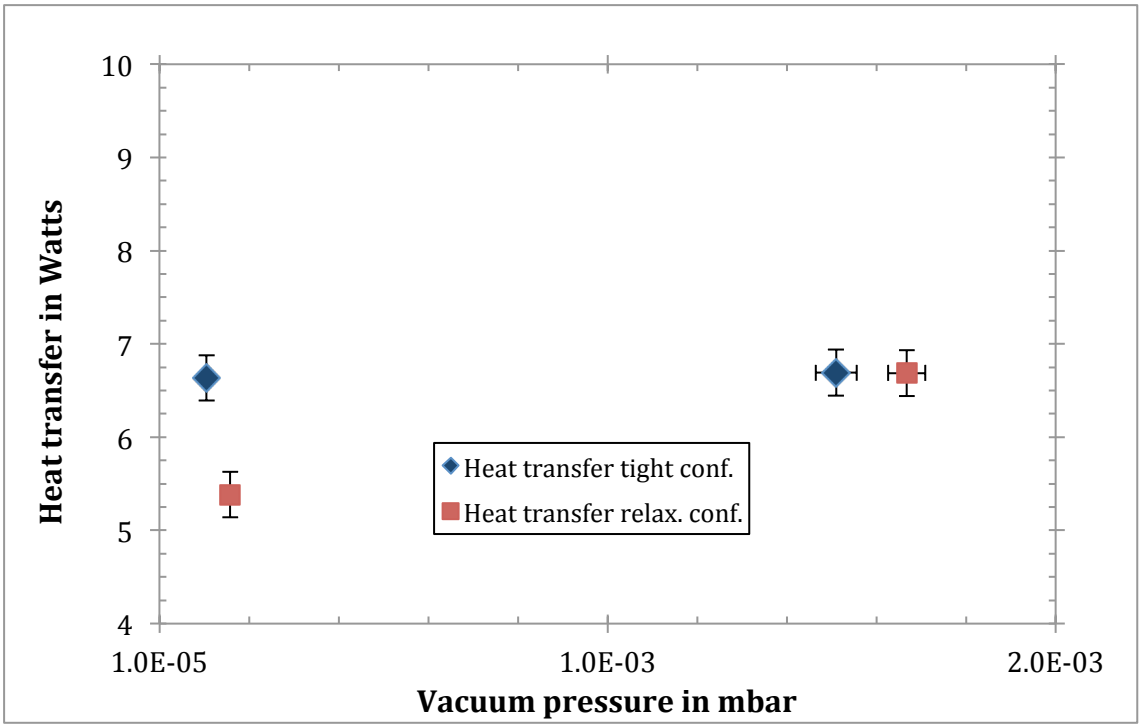


Figure 7-11 Heat transfer during the measurements in coiled - tight and coiled - relaxed configuration of the transfer line at different vacuum pressures with the coolant temperature measured at the inlet = -40°C and mass flow rate = 6g/s.

Figure 7-11 provides information about the heat transfer during the measurement in coiled-tight and coiled-relaxed configuration. The heat transfer has increased in comparison to the straight configuration. The lowest value and the only value different from the rest of the measurements is for coiled – relaxed configuration at a good vacuum level. The reduced heat transfer by conduction in this scenario resulted in a lower value.

Figure 7-12 represents temperature differences between ambient and surface temperatures of the transfer line in coiled – tight and coiled – relaxed configuration. It can be observed that the values depicted are much higher than in a straight configuration.

The greatest temperature difference was measured on the cold spot of the transfer line at the worse vacuum level in coiled – tight configuration. In this case the force exerted by the inner pipe of the transfer line on the outer hose was the greatest. Therefore, it can be assumed that this configuration is the worst case scenario and the temperature difference should never be higher than in this case, with the bending radius of the transfer line equal or greater than 5 cm.

The values obtained for coiled – tight and coiled – relaxed configuration show a slight decrease in temperature differences for coiled – relaxed configuration. Nevertheless, they stay in relatively the same range.

The greatest difference in obtained values can be observed between cold spots and reference points on the transfer line. It is worth mentioning that in coiled configuration even the reference points temperature was slightly lower which can be deducted by analysing their temperature differences with ambient temperatures.

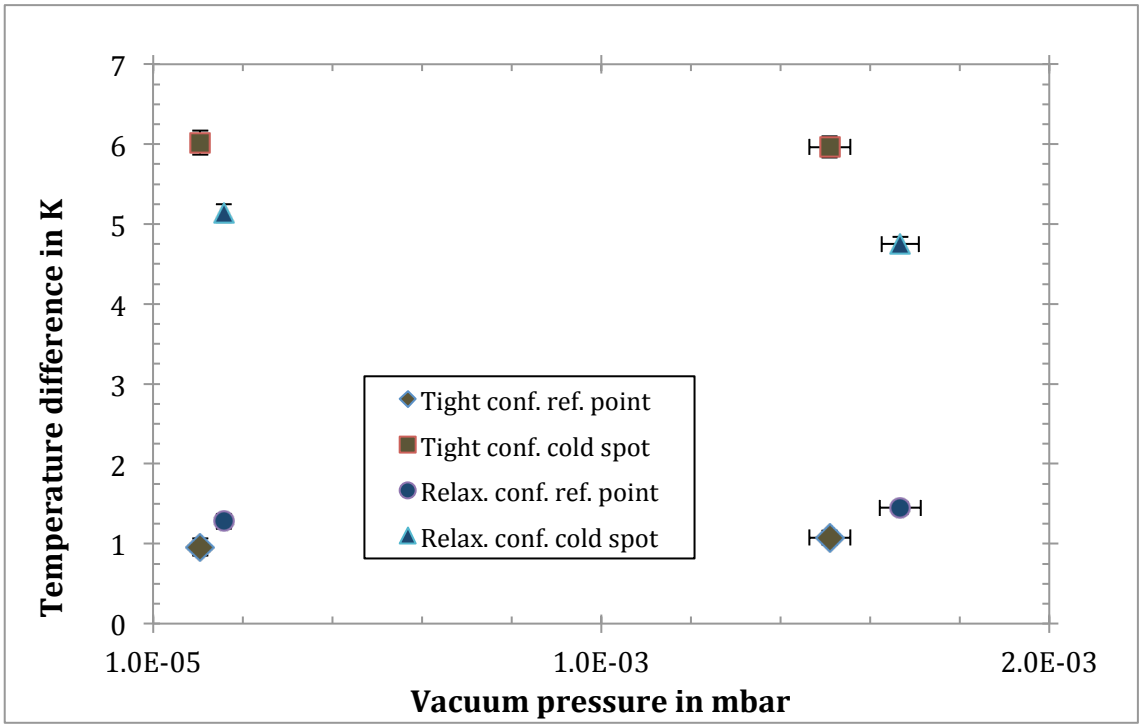


Figure 7-12 Temperature difference between ambient and surface temperature measured on the flexible part of the transfer line in coiled - tight and coiled - relaxed configuration of the transfer line at different vacuum pressures with the coolant temperature measured at the inlet = -40°C and mass flow rate = 6g/s.

Table 7.4 presents infrared pictures of the transfer line taken during the measurements in coiled – tight configuration of the transfer line. It can be observed how big the impact of the contact of the transfer line inner pipe with the outer hose is.

In straight configuration of the transfer line it was difficult to localize even one cold spot, whereas in this scenario there are more of them and their negative influence on the performance of the transfer line is noticeable. Nevertheless, they still should not lead to the condensation on the surface of the transfer line with the ambient conditions inside of the ATLAS experiment cavern.

Based on Table 7.4 it can be observed that the surface temperatures were higher with the worse vacuum pressure. However, it remains true only for this particular measurement as ambient conditions had this specific influence. Based on Table 7.5 one is no longer able to draw such a conclusion as the results are just opposite. The environment influences in this case turned out to be once again greater than the measurement accuracy.

As observed on Table 7.4 and Table 7.5 cold spots now constitute to a relatively large part of the surface area. In order to prevent this kind of situation in the future a lot of caution has to be taken while bending the transfer line. In this case the transfer line was bent rather spontaneously, therefore the inner pipe can be bent to excessively insight which led to a creation of large number of cold spots. The performance of the transfer line can be further improved provided that enough care is taken while setting up of the system.

Table 7.4: IR pictures taken on four different spots of the transfer line during the measurements in coiled - tight configuration of the transfer line at different vacuum pressures with the coolant temperature measured at the inlet = -40°C and mass flow rate = 6g/s.

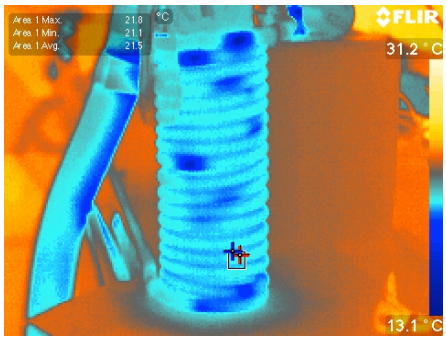
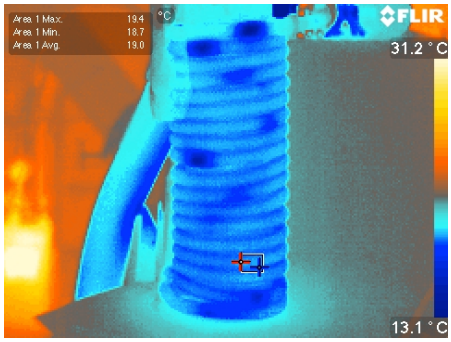
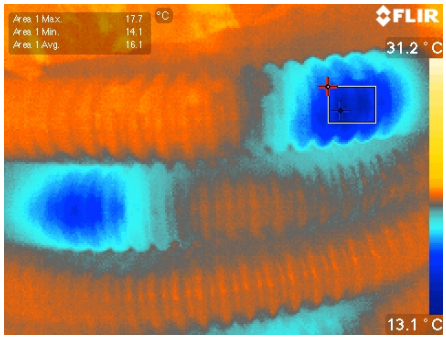
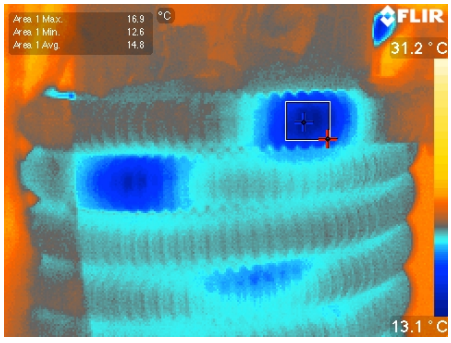
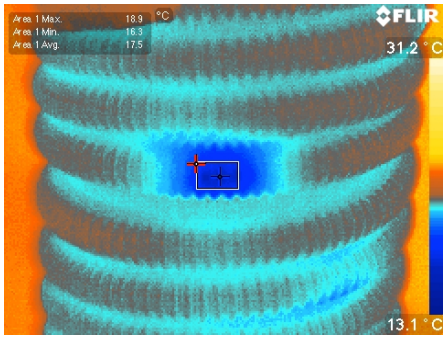
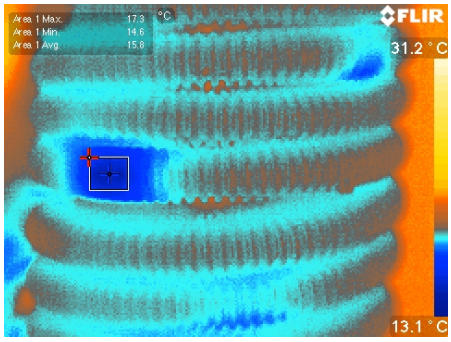
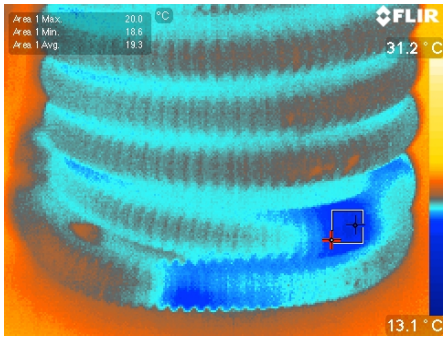
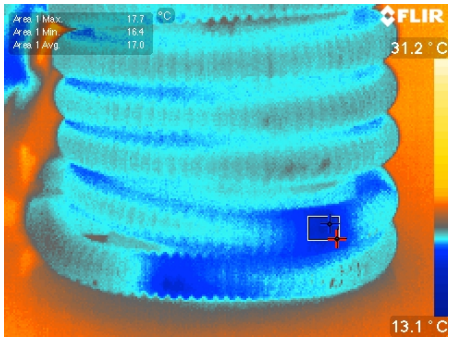
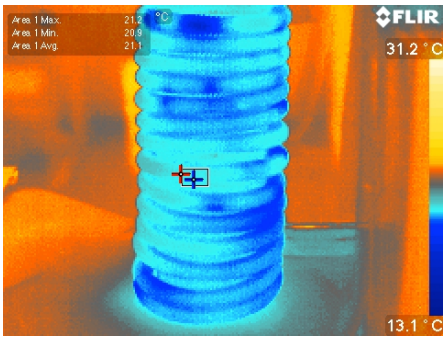
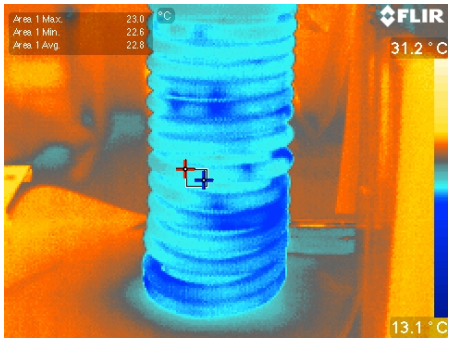
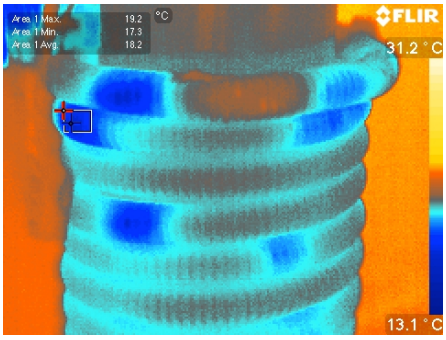
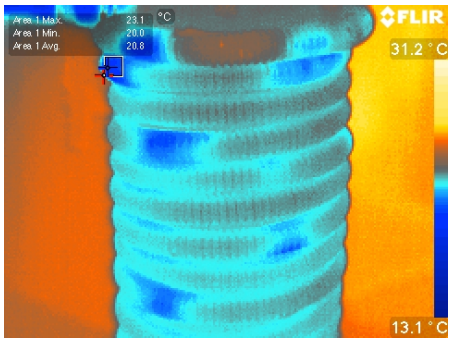
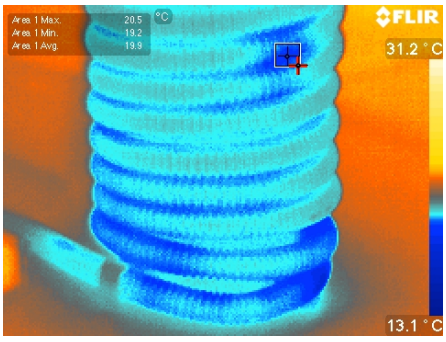
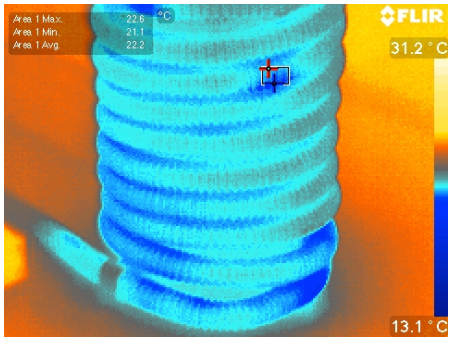
Vacuum pressure	$1.2x10^{-4}$ [mbar]	$1.4x10^{-3}$ [mbar]
Reference Point		
	t_{avg}= 21.5°C	t_{avg}= 19.0°C
Top cold spot		
	t_{avg}= 16.1°C	t_{avg}= 14.8°C
Middle cold spot		
	t_{avg}= 17.5°C	t_{avg}= 15.8°C
Bottom cold spot		
	t_{avg}= 19.3°C	t_{avg}= 17.0°C

Table 7.5: IR pictures taken on four different spots of the transfer line during the measurements in coiled - relaxed configuration at different vacuum pressures with the coolant temperature measured at the inlet = -40°C and mass flow rate = 6g/s.

Vacuum pressure	$1.8x10^{-4}$ [mbar]	$1.6x10^{-3}$ [mbar]
Reference Point	 t_{avg}= 21.1°C	 t_{avg}= 22.8°C
Top cold spot	 t_{avg}= 18.2°C	 t_{avg}= 20.8°C
Bottom cold spot	 t_{avg}= 19.9°C	 t_{avg}= 22.2°C

7.3 Bent rigid part of the transfer line

Bent rigid part of the transfer line was a special measurement, which aimed at observing the behaviour of the transfer line in coiled configuration with its rigid part bent at 90 degrees angle. This test was performed at different vacuum pressure levels with coolant temperature measured at the inlet kept at -40 °C. Mass flow rate was 6 g/s.

Figure 7-13 depicts temperature differences between the outlet and the inlet of the transfer line with its rigid part being bent. It can be observed that the temperature difference increases at worse vacuum level and does not exceed 1.5 ± 0.04 K. The precise influence of the created bent

on the performance of the transfer line is difficult to determine, as flexible part was coiled and it had a major impact on the obtained values.

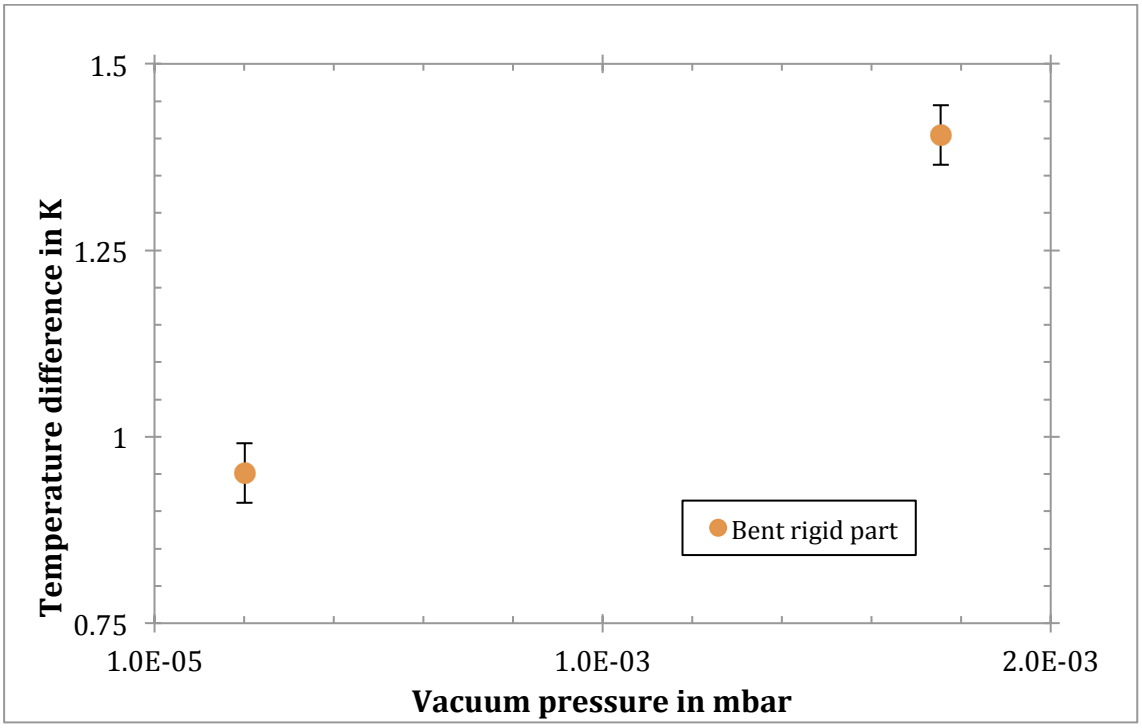


Figure 7-13 Temperature difference between outlet and inlet of the transfer line measured after the bending of the rigid part of the transfer line at different vacuum pressures with the coolant temperature measured at the inlet = -40°C.

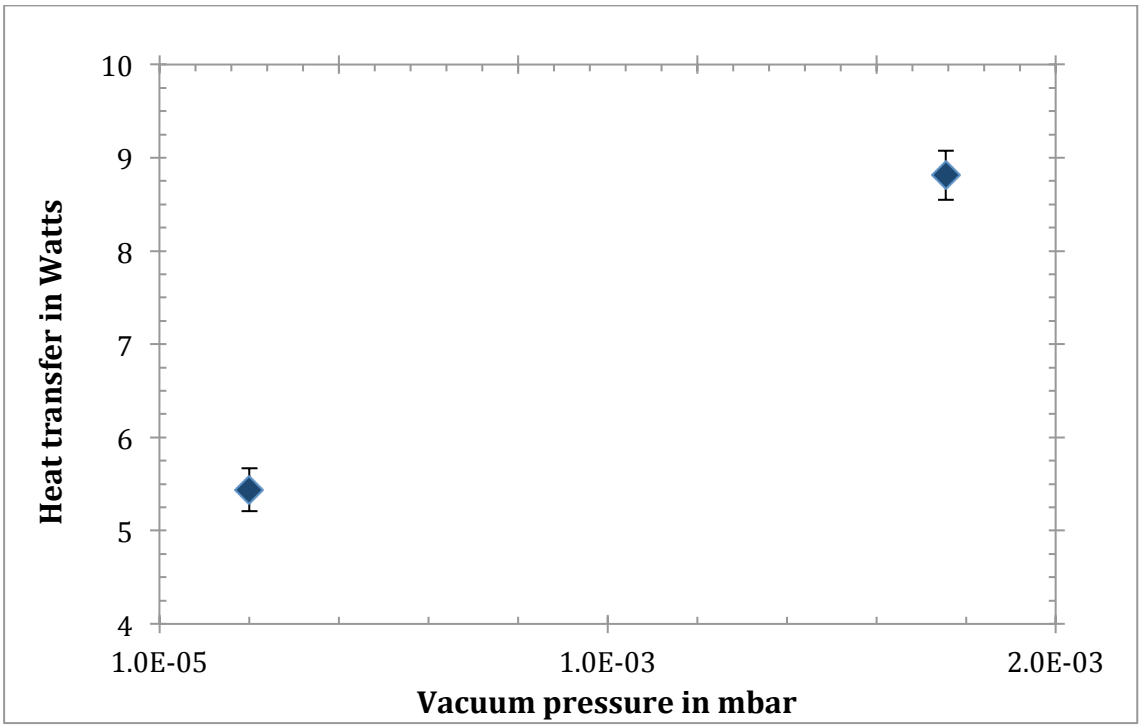


Figure 7-14 Heat transfer depending on vacuum pressure during the measurement after the bending of the rigid part of the transfer line wit the coolant temperature measured at the inlet = -40°C.

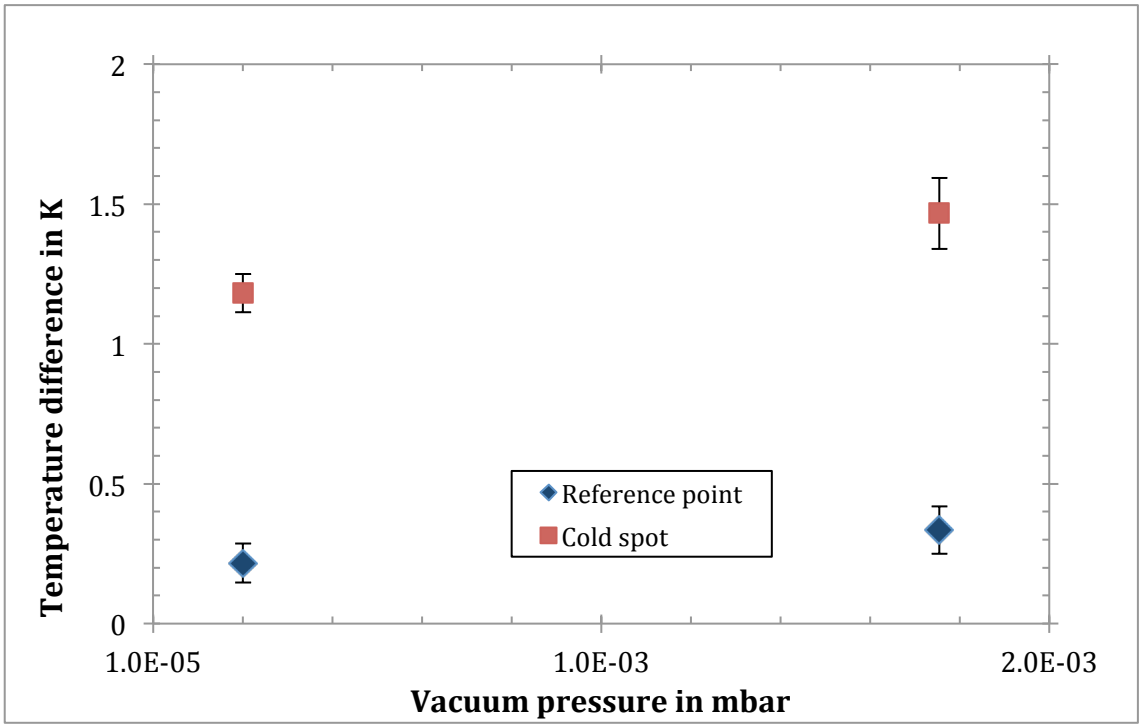
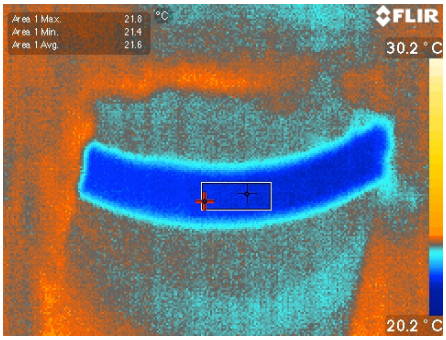
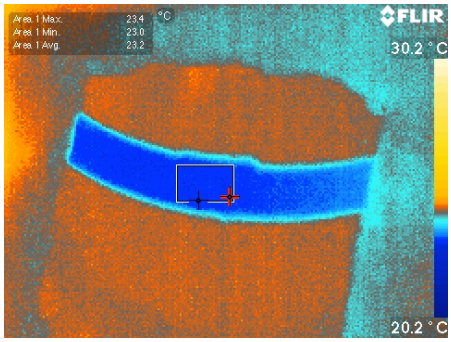


Figure 7-15 Temperature difference between ambient and surface temperature measured on the rigid part of the transfer after bending of it at different vacuum pressures.

Figure 7-14 depicts heat transfer values depending on vacuum pressure levels. As expected after observing temperature differences between the outlet and the inlet of the transfer line the value for the worse vacuum level is higher than at the good vacuum level.

Figure 7-15 provides very important information about the temperature difference between the ambient and the surface temperature of the transfer line. It can be observed that in this case the values obtained are in range of those from straight configuration rather than coiled – tight configuration of the transfer line. This may be a result of a lot of precaution taken during the bending process of the transfer line. Table 7.6 shows no cold spots on the bend itself.

Table 7.6: IR pictures taken on four different spots of the transfer line during the measurements of the bent rigid part at different vacuum pressures

Vacuum pressure	1.9×10^{-4} [mbar]	1.8×10^{-3} [mbar]
Reference Point 1		
	t_{avg}= 21.6°C	t_{avg}= 23.2°C

8 Conclusions

The aim of this thesis was to determine whether the design of the CO_2 flexible vacuum insulated transfer line proposed by Dr Thomas Eisel can be used for the supply and return line of the ATLAS IBL Detector Cooling System.

For the purposes of this experiment a close to full-scale mock-up of the transfer line was built and tested with the usage of C_6F_{14} as a coolant. The thermodynamic performance of the transfer line has been investigated in three different configurations and all of them delivered positive results that comply with the IBL Cooling System requirements.

The values measured included mass flow rate, vacuum pressure, surface and ambient temperatures as well as temperature of the coolant at the inlet and outlet of the transfer line. Appropriate temperature differences were calculated and compared in and across different measurement scenarios. The same sets of comparisons were performed for the heat transfer values and information deducted from the IR pictures.

According to the expectations, the transfer line achieved the best thermal performance in the straight configuration, where no bending was applied to any of its parts. The highest temperature differences between ambient and surface temperatures in this configuration stayed within the range of 0.46 ± 0.11 K and 0.56 ± 0.11 K and were observed during the measurements at worse vacuum level at the coolant temperature equal to -40°C. On the contrary, the lowest temperature differences were observed within the range of 0.16 K ± 0.11 K and 0.29 K ± 0.11 K while measured during the test in which the coolant temperature was the highest -20°C.

The temperature differences between the coolant temperatures measured at the outlet and inlet of the transfer line in the straight configuration were the lowest of all the measurements and did not exceed 0.79 K ± 0.04 K. Additionally, the temperature gradients observed with the IR camera were as well the lowest and the heat transfer rate did not exceed 5 Watt.

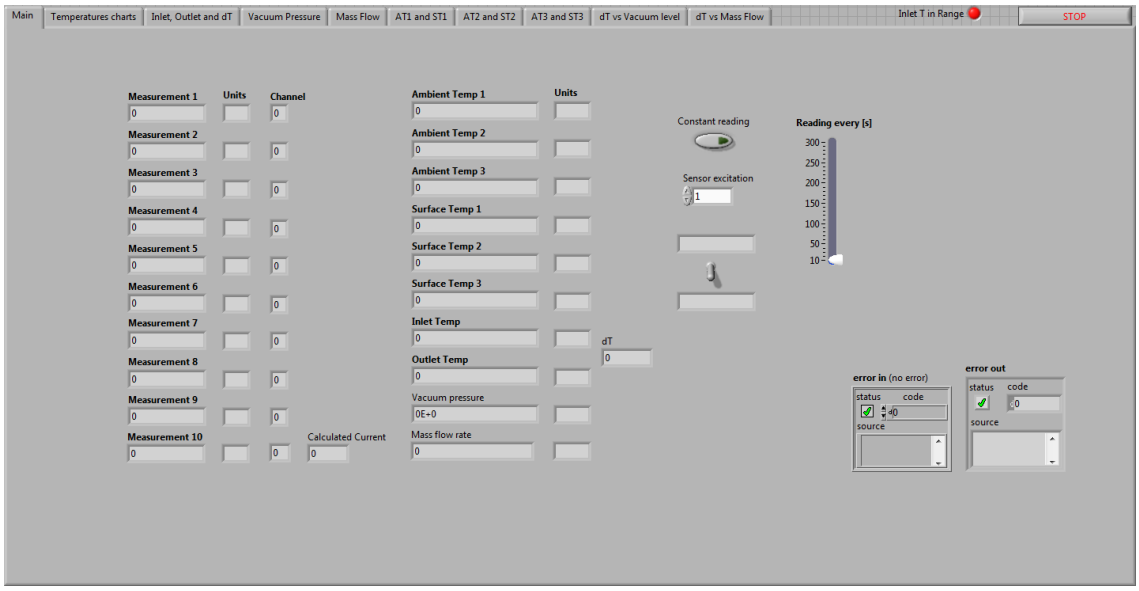
Measurements in the bent – tight and bent – relaxed configurations provided the highest temperature differences between ambient and surface temperatures and the greatest temperature gradients on the surface of the transfer line. The temperature differences between ambient and cold spot temperatures reached 6.02 ± 0.15 K and 5.13 ± 0.11 K for tight and relaxed configuration respectively at a coolant temperature measured at the inlet equal to -40°C. Taking into account that the temperature in the ATLAS experiment cavern where the transfer line is supposed to be installed ranges from 20 to 25°C - there is at least 4 ± 0.15 K safety margin from the dew point which is less than 10°C. Due to the fact that these configurations were the worst-case scenarios it is assumed that the transfer line investigated and described in this thesis can be safely used for the ATLAS IBL Detector Cooling System.

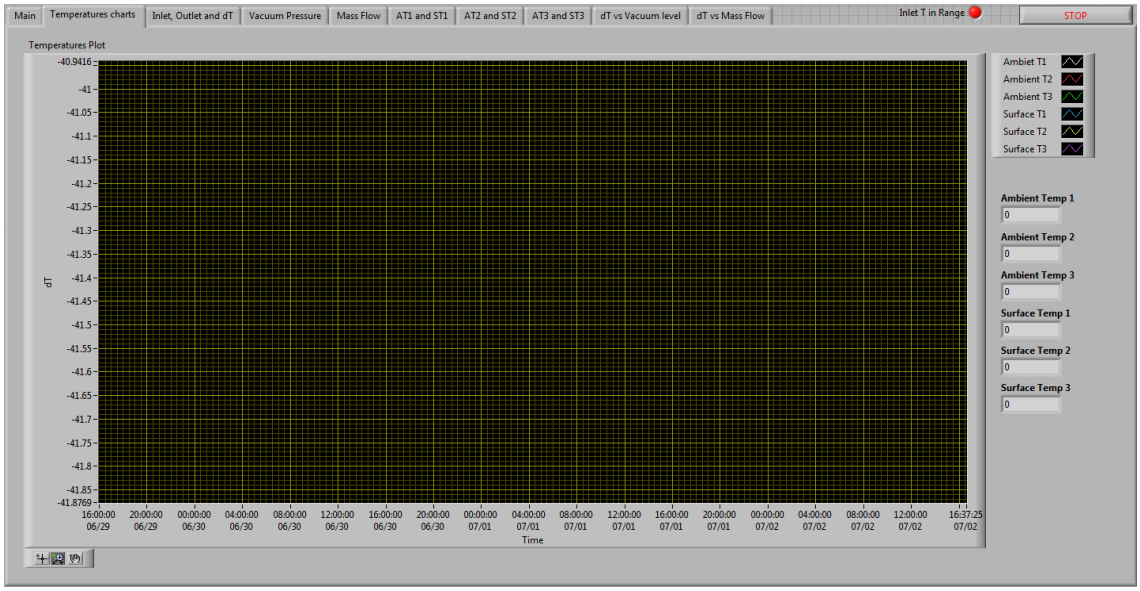
Additional research on the thermal performance of the transfer line included bending of the rigid pipe of the transfer line at 90° angle. In this case temperature differences at different vacuum pressures between localised cold spot and ambient temperatures did not exceed 1.47 ± 0.13 K. As a result it is concluded that not only the flexible part of the transfer line can be bend but also the rigid part may be exposed to bending without a significant increase in heat inleak.

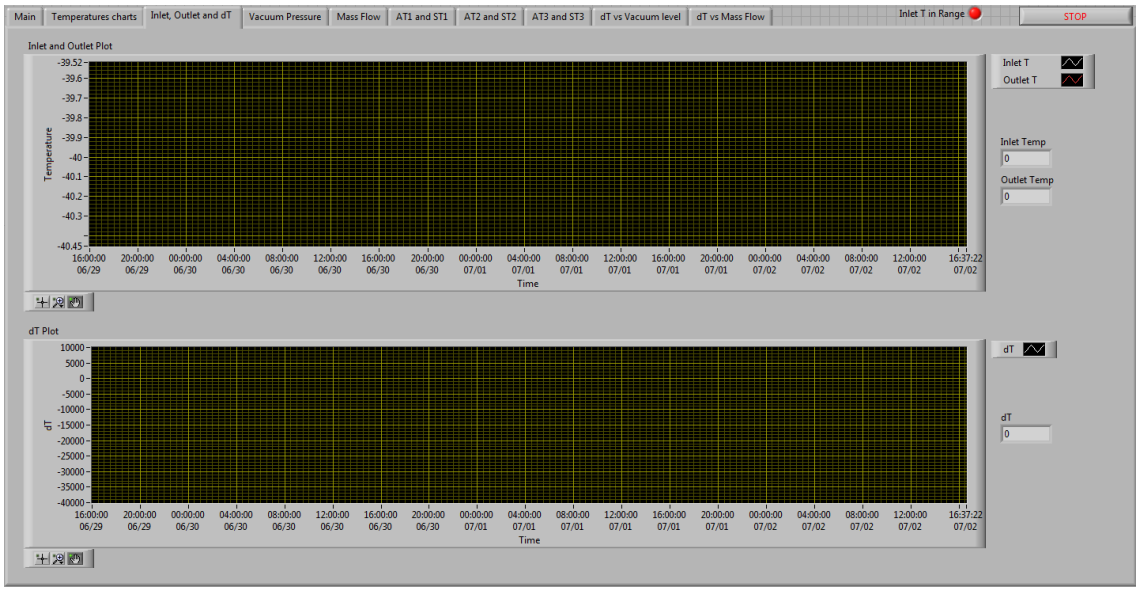
In conclusion, the transfer line performed well from the thermodynamic point of view in all of the measuring configurations. There was no evidence found that would prevent this technology from being installed in the ATLAS experiment cavern.

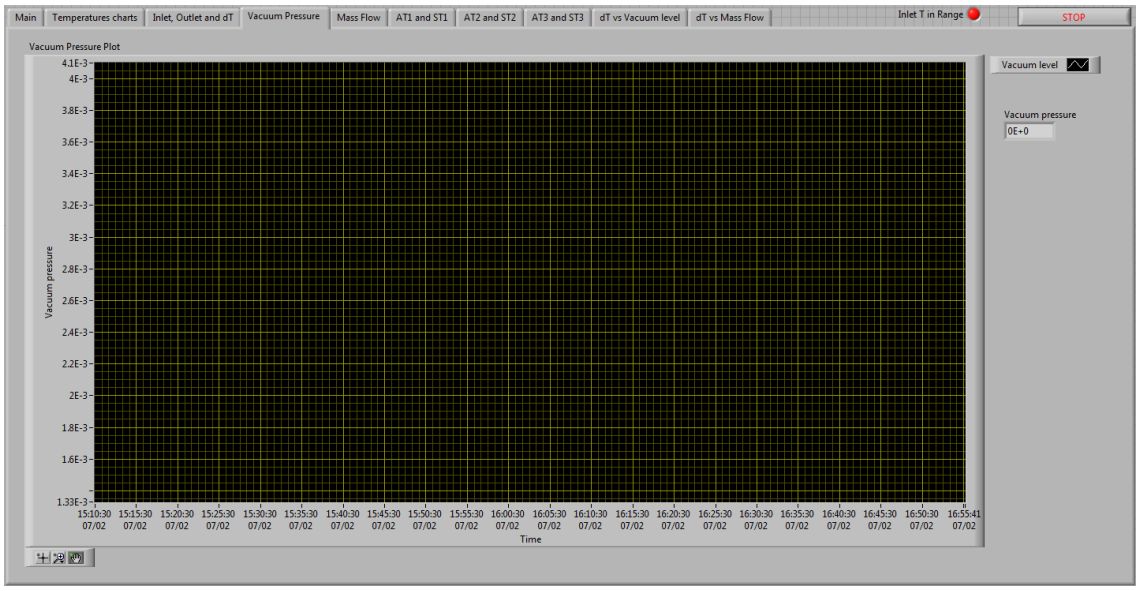
Appendices

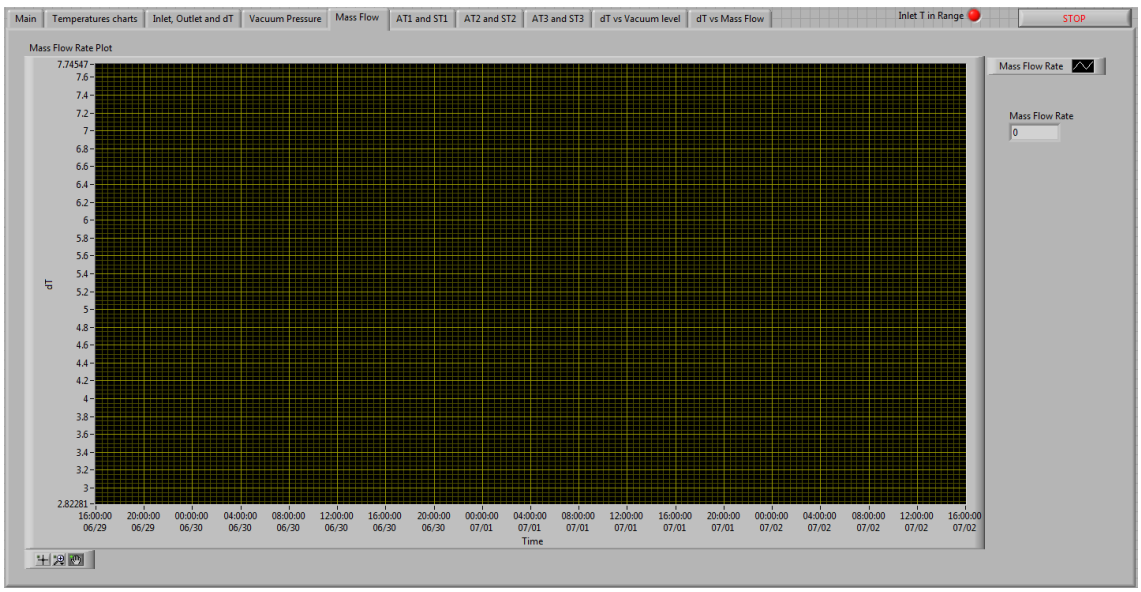
Below is presented Graphical User Interface of the LabVIEW program created for the purposes of the experiment with its block diagram.

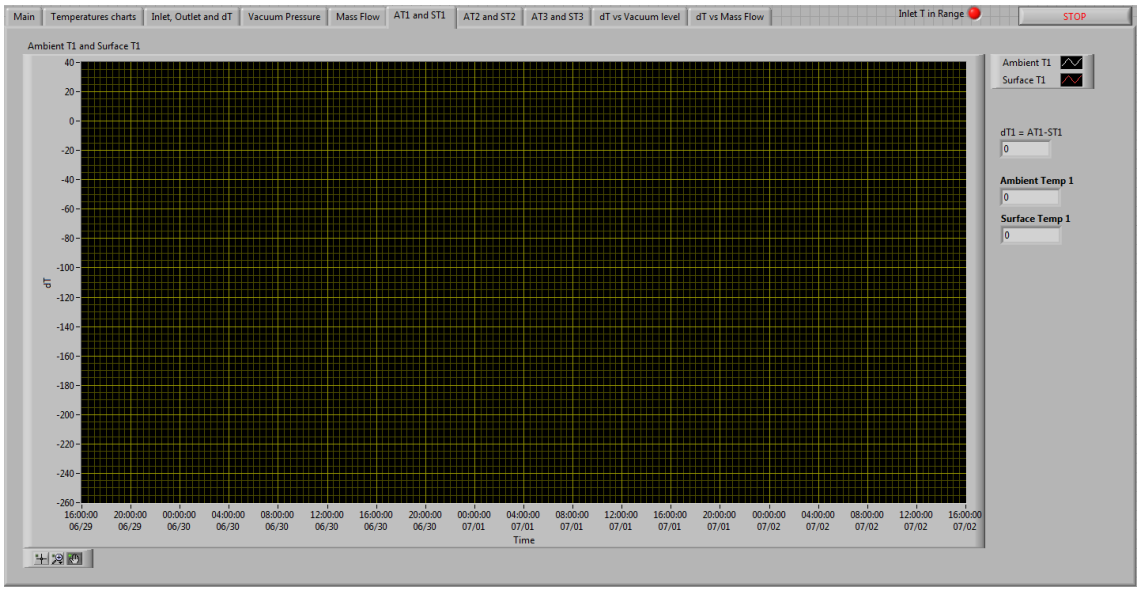


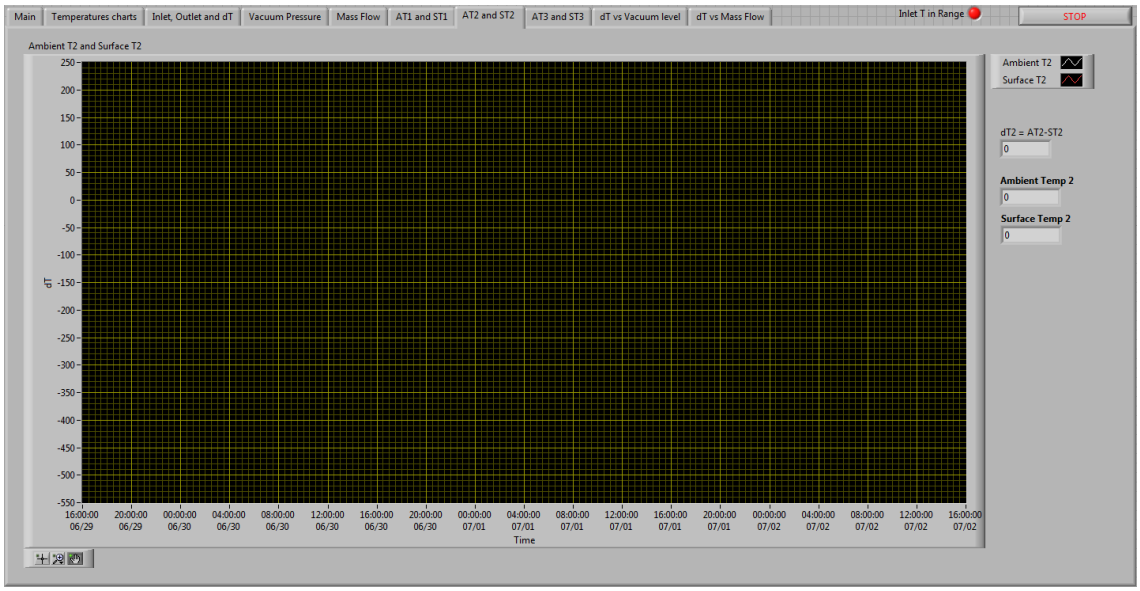


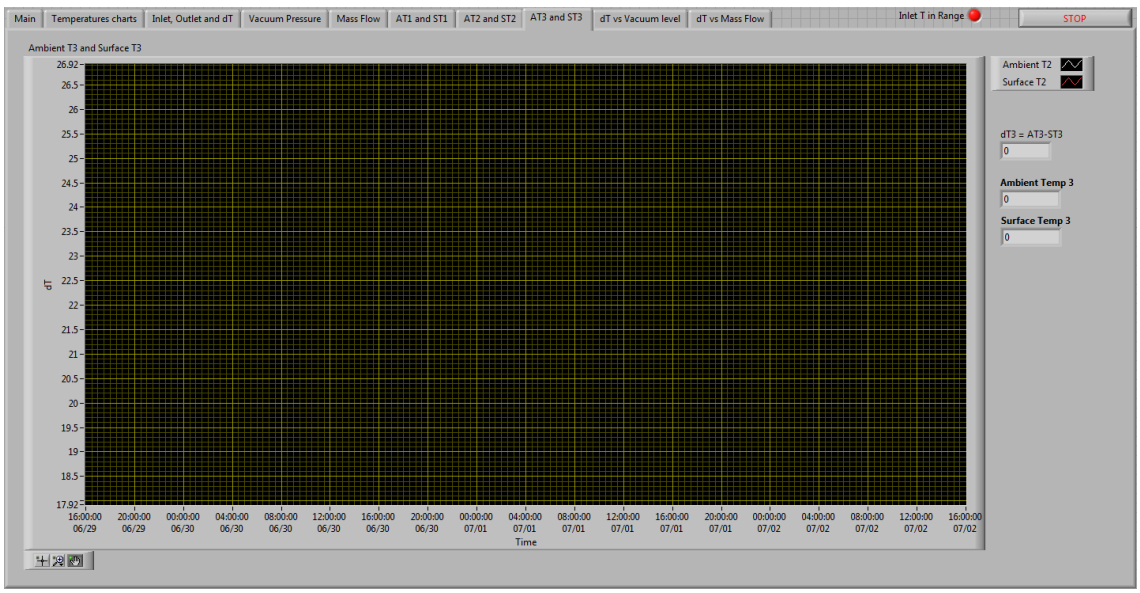

Main
Temperatures charts
Inlet, Outlet and dT
Vacuum Pressure
Mass Flow
AT1 and ST1
AT2 and ST2
AT3 and ST3
dT vs Vacuum level
dT vs Mass Flow
Inlet T in Range
STOP
Inlet and Outlet Plot
Temperature
Time
Inlet T
Outlet T
Inlet Temp
Outlet Temp
dT Plot
dT

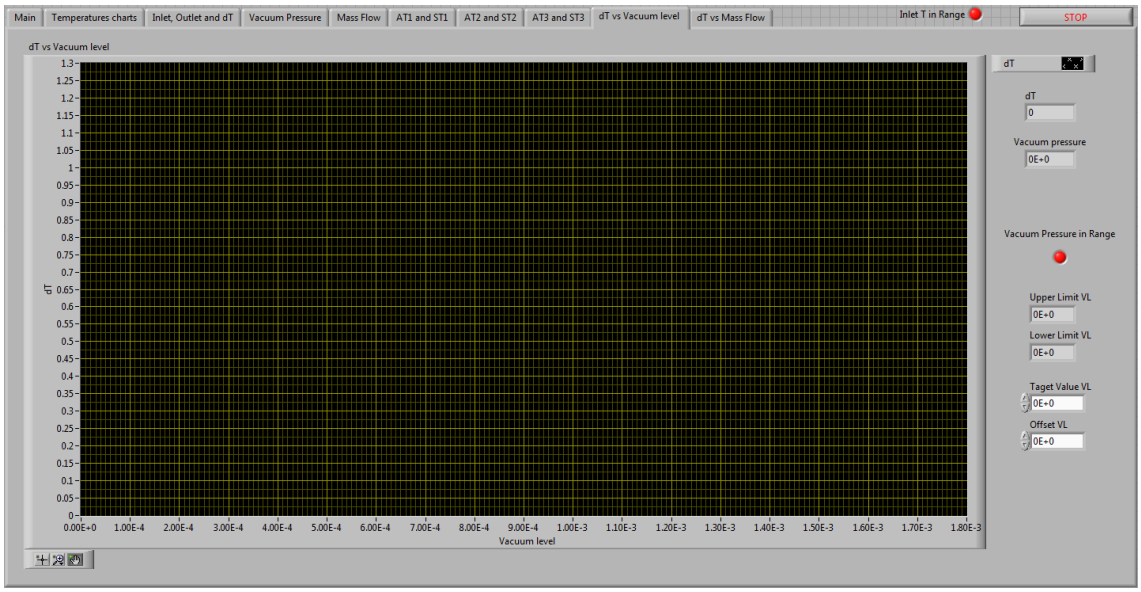

Main
Temperatures charts
Inlet, Outlet and dT
Vacuum Pressure
Mass Flow
AT1 and ST1
AT2 and ST2
AT3 and ST3
dT vs Vacuum level
dT vs Mass Flow
Inlet T in Range
STOP
Vacuum Pressure Plot
Vacuum pressure
Time
Vacuum level
Vacuum pressure

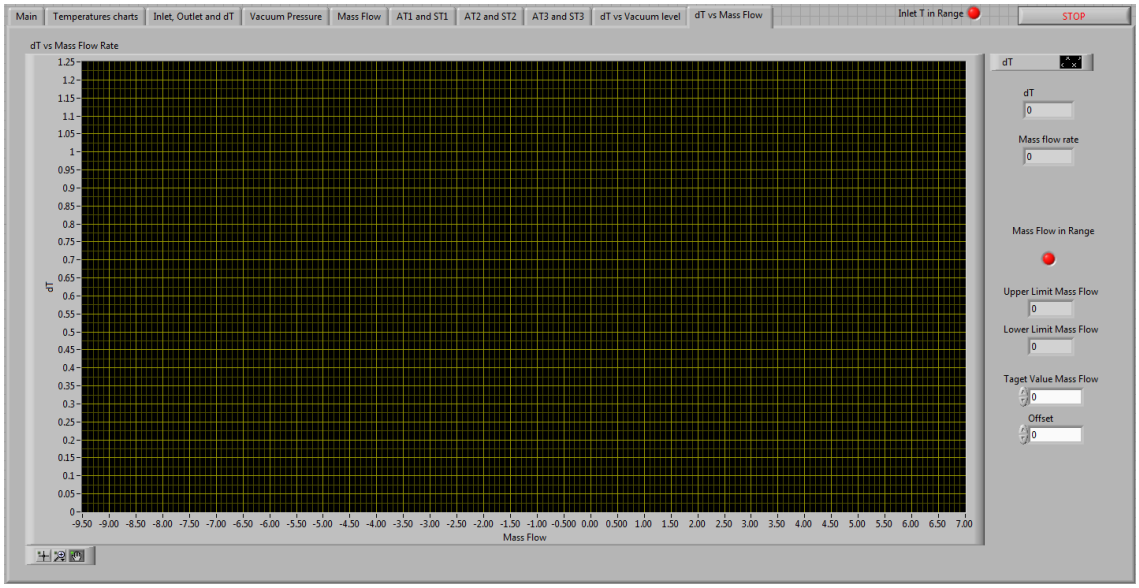

Main
Temperatures charts
Inlet, Outlet and dT
Vacuum Pressure
Mass Flow
AT1 and ST1
AT2 and ST2
AT3 and ST3
dT vs Vacuum level
dT vs Mass Flow
Inlet T in Range
STOP
Mass Flow Rate Plot
dT
Time
Mass Flow Rate
Mass Flow Rate

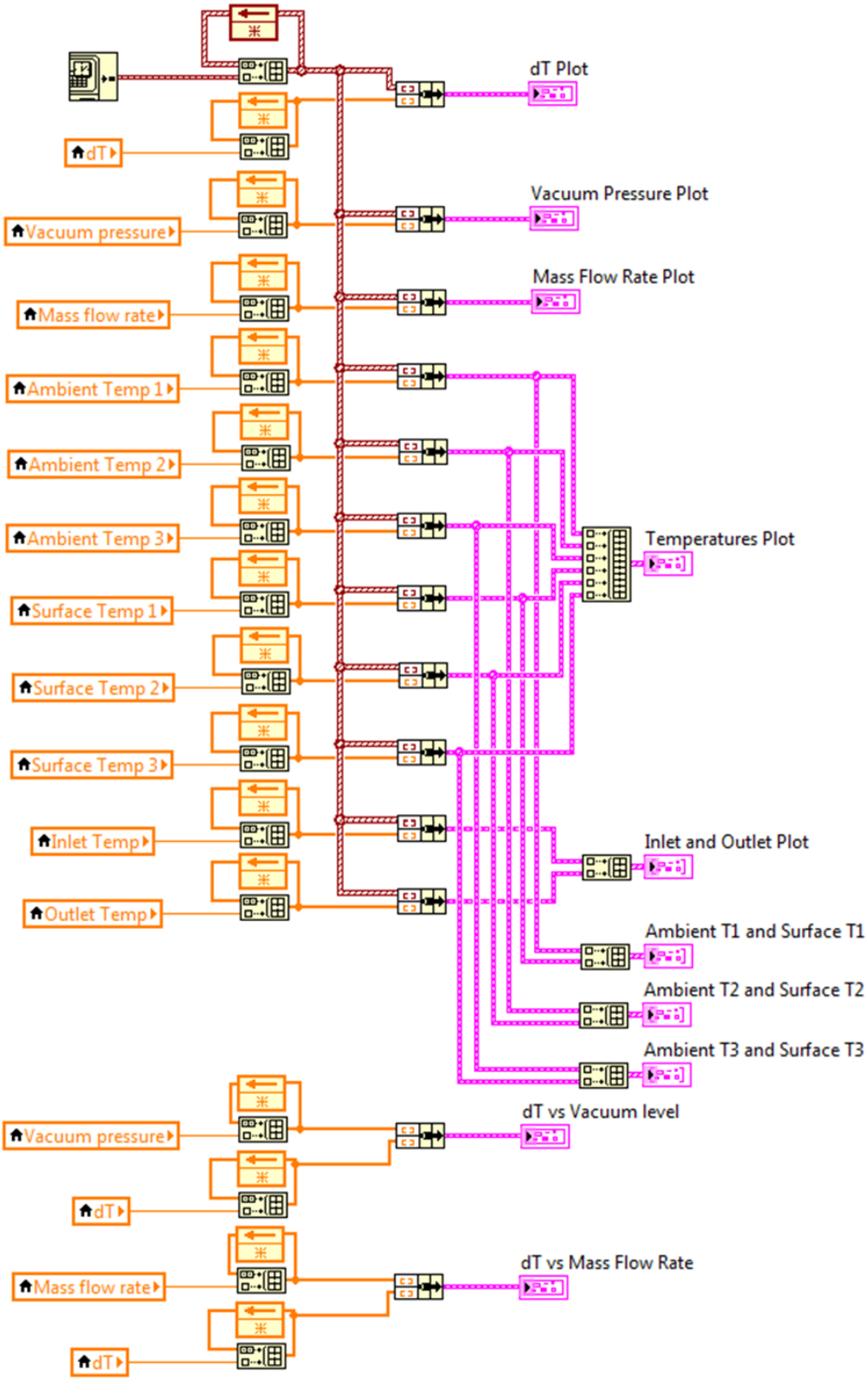

Main
Temperatures charts
Inlet, Outlet and dT
Vacuum Pressure
Mass Flow
AT1 and ST1
AT2 and ST2
AT3 and ST3
dT vs Vacuum level
dT vs Mass Flow
Inlet T in Range
STOP
Ambient T1 and Surface T1
dT
Time
Ambient T1
Surface T1
dT1 = AT1-ST1
Ambient Temp 1
Surface Temp 1

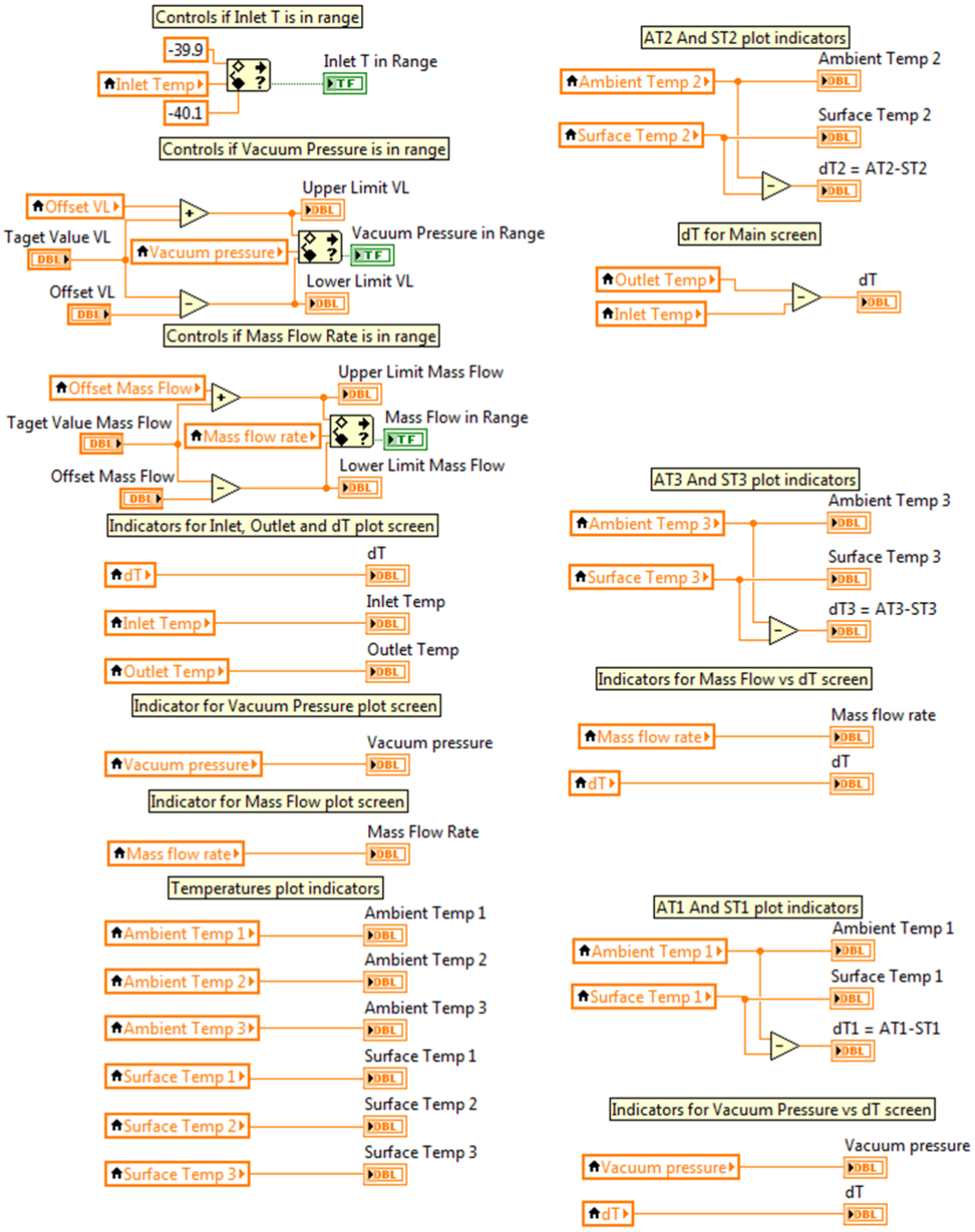

Main
Temperatures charts
Inlet, Outlet and dT
Vacuum Pressure
Mass Flow
AT1 and ST1
AT2 and ST2
AT3 and ST3
dT vs Vacuum level
dT vs Mass Flow
Inlet T in Range
STOP
Ambient T2 and Surface T2
dT
Time
Ambient T2
Surface T2
dT2 = AT2-ST2
Ambient Temp 2
Surface Temp 2

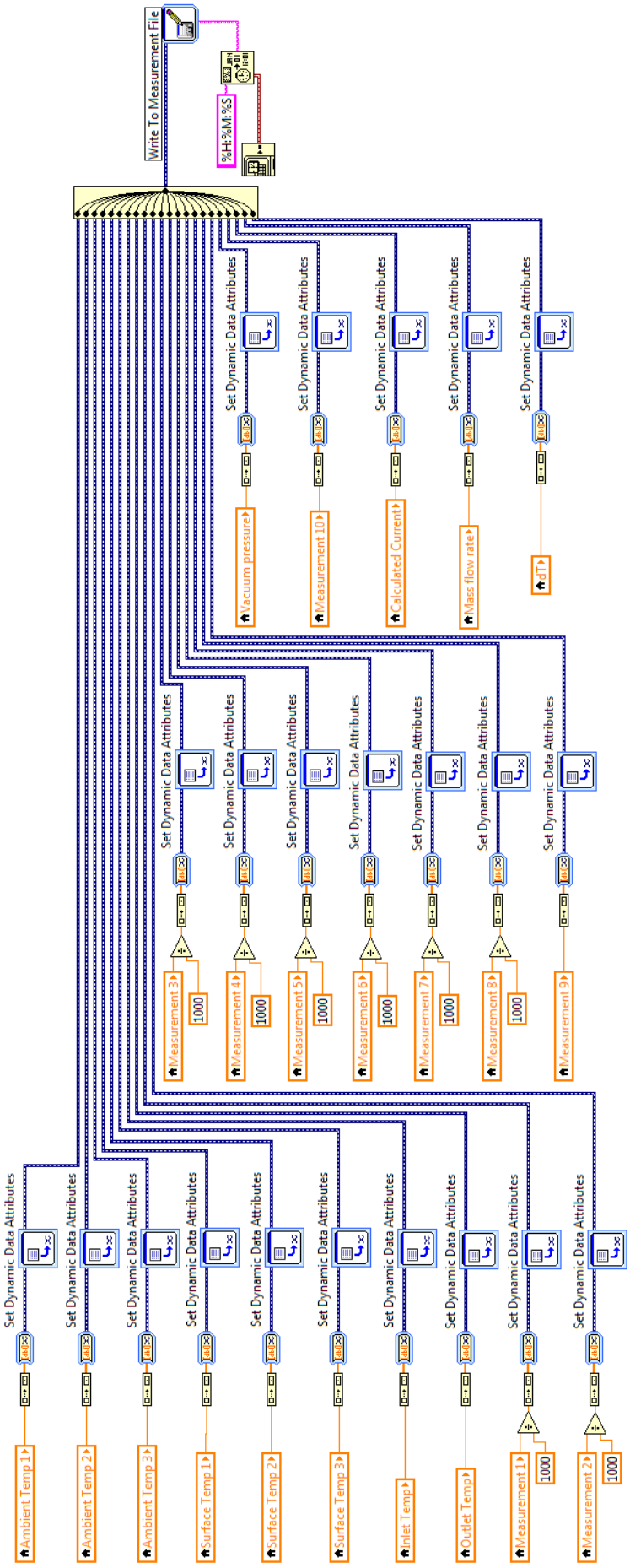

Main
Temperatures charts
Inlet, Outlet and dT
Vacuum Pressure
Mass Flow
AT1 and ST1
AT2 and ST2
AT3 and ST3
dT vs Vacuum level
dT vs Mass Flow
Inlet T in Range
STOP
Ambient T3 and Surface T3
dT
Time
Ambient T2
Surface T2
dT3 = AT3-ST3
Ambient Temp 3
Surface Temp 3

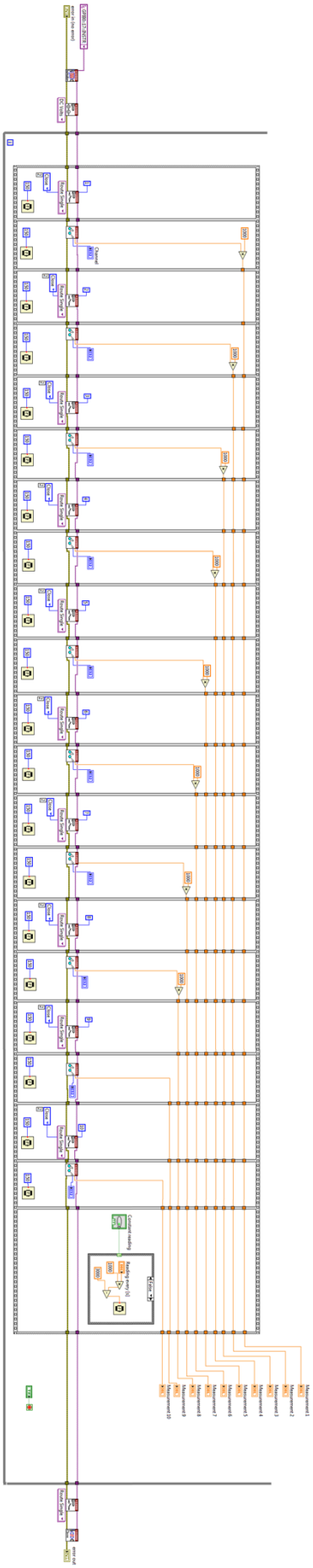

Main
Temperatures charts
Inlet, Outlet and dT
Vacuum Pressure
Mass Flow
AT1 and ST1
AT2 and ST2
AT3 and ST3
dT vs Vacuum level
dT vs Mass Flow
Inlet T in Range
STOP
dT vs Vacuum level
dT
Vacuum level
dT
Vacuum pressure
Vacuum Pressure in Range
Upper Limit VL
Lower Limit VL
Taget Value VL
Offset VL

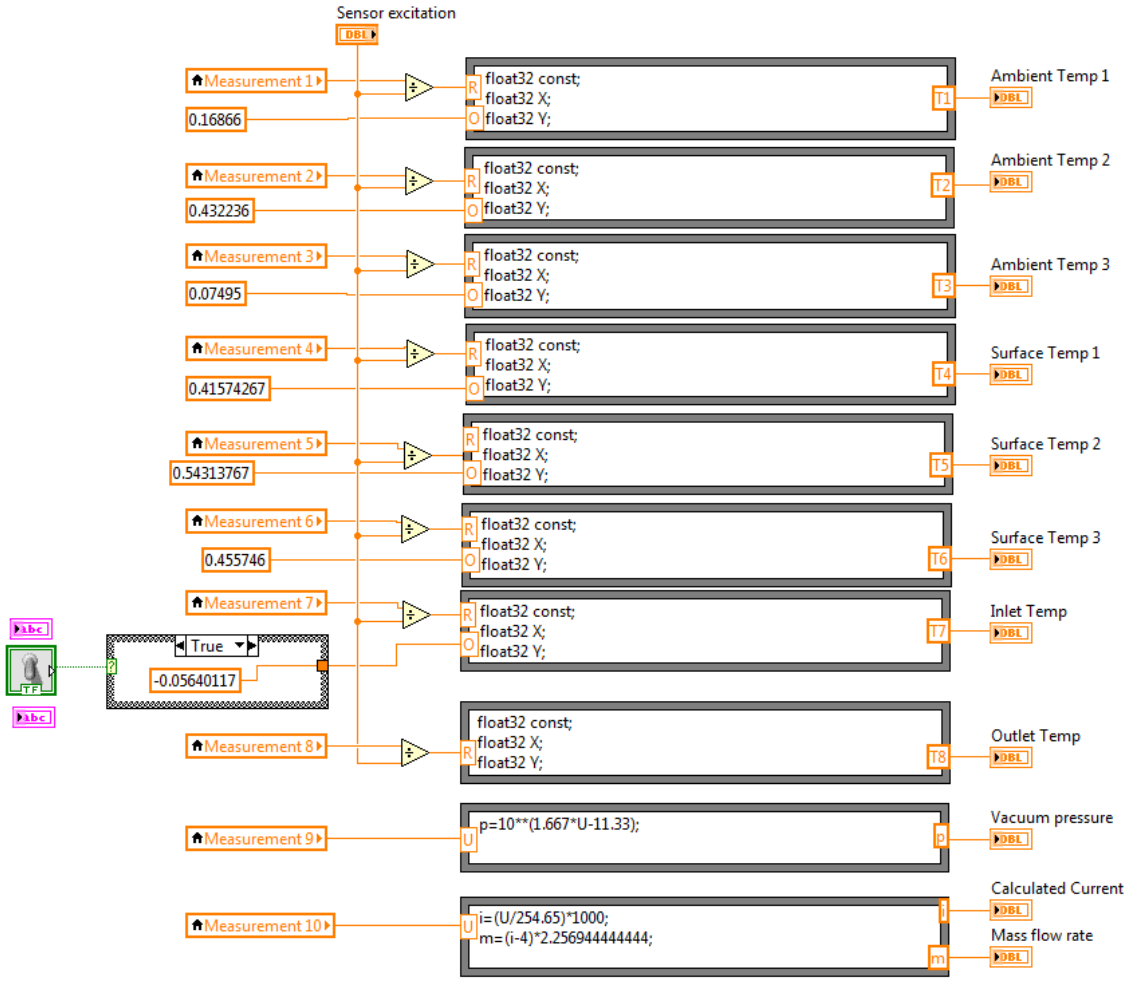

Main
Temperatures charts
Inlet, Outlet and dT
Vacuum Pressure
Mass Flow
AT1 and ST1
AT2 and ST2
AT3 and ST3
dT vs Vacuum level
dT vs Mass Flow
Inlet T in Range
STOP
dT vs Mass Flow Rate
dT
Mass Flow
dT
Mass flow rate
Mass Flow in Range
Upper Limit Mass Flow
Lower Limit Mass Flow
Taget Value Mass Flow
Offset


dT Plot
dT
Vacuum Pressure Plot
Vacuum pressure
Mass Flow Rate Plot
Mass flow rate
Ambient Temp 1
Ambient Temp 2
Ambient Temp 3
Surface Temp 1
Surface Temp 2
Surface Temp 3
Temperatures Plot
Inlet Temp
Outlet Temp
Inlet and Outlet Plot
Ambient T1 and Surface T1
Ambient T2 and Surface T2
Ambient T3 and Surface T3
Vacuum pressure
dT vs Vacuum level
dT
Mass flow rate
dT vs Mass Flow Rate
dT


Controls if Inlet T is in range
-39.9
Inlet T in Range
Inlet Temp
TF
-40.1
Controls if Vacuum Pressure is in range
Upper Limit VL
Offset VL
Taget Value VL
Vacuum Pressure in Range
Vacuum pressure
TF
Lower Limit VL
Offset VL
Controls if Mass Flow Rate is in range
Upper Limit Mass Flow
Offset Mass Flow
Taget Value Mass Flow
Mass Flow in Range
Mass flow rate
TF
Lower Limit Mass Flow
Offset Mass Flow
Indicators for Inlet, Outlet and dT plot screen
dT
dT
Inlet Temp
Inlet Temp
Outlet Temp
Outlet Temp
Indicator for Vacuum Pressure plot screen
Vacuum pressure
Vacuum pressure
Indicator for Mass Flow plot screen
Mass Flow Rate
Mass flow rate
Temperatures plot indicators
Ambient Temp 1
Ambient Temp 1
Ambient Temp 2
Ambient Temp 2
Ambient Temp 3
Ambient Temp 3
Surface Temp 1
Surface Temp 1
Surface Temp 2
Surface Temp 2
Surface Temp 3
Surface Temp 3
AT2 And ST2 plot indicators
Ambient Temp 2
Ambient Temp 2
Surface Temp 2
Surface Temp 2
dT2 = AT2-ST2
dT for Main screen
Outlet Temp
dT
Inlet Temp
AT3 And ST3 plot indicators
Ambient Temp 3
Ambient Temp 3
Surface Temp 3
Surface Temp 3
dT3 = AT3-ST3
Indicators for Mass Flow vs dT screen
Mass flow rate
Mass flow rate
dT
dT
AT1 And ST1 plot indicators
Ambient Temp 1
Ambient Temp 1
Surface Temp 1
Surface Temp 1
dT1 = AT1-ST1
Indicators for Vacuum Pressure vs dT screen
Vacuum pressure
Vacuum pressure
dT
dT


Write To Measurement File
%H:%M:%S
Set Dynamic Data Attributes
Vacuum pressure
Measurement 10
Calculated Current
Mass flow rate
dT
Measurement 3
Measurement 4
Measurement 5
Measurement 6
Measurement 7
Measurement 8
Measurement 9
1000
Ambient Temp 1
Ambient Temp 2
Ambient Temp 3
Surface Temp 1
Surface Temp 2
Surface Temp 3
Inlet Temp
Outlet Temp
Measurement 1
Measurement 2




Sensor excitation
Measurement 1
0.16866
Measurement 2
0.432236
Measurement 3
0.07495
Measurement 4
0.41574267
Measurement 5
0.54313767
Measurement 6
0.455746
Measurement 7
Measurement 8
Measurement 9
Measurement 10
float32 const;
float32 X;
float32 Y;
Ambient Temp 1
Ambient Temp 2
Ambient Temp 3
Surface Temp 1
Surface Temp 2
Surface Temp 3
Inlet Temp
Outlet Temp
p=10**(1.667*U-11.33);
Vacuum pressure
i=(U/254.65)*1000;
m=(i-4)*2.256944444444;
Calculated Current
Mass flow rate
True
-0.05640117

List of references

[1] CERN. [Online]. http://home.web.cern.ch/about

[2] ATLAS IBL Community, "Insertable B-Layer Technical Design Report," LHCC, CERN, 2010.

[3] Bart Verlaat, "Piping and Instrumentation for the Atlas IBL CO2 cooling system," Physics Department, CERN, 2012.

[4] Sven Vogt, Thomas Eisel, Marek Gutt-Mostowy, Jan Godlewski, Łukasz Zwaliński Bart Verlaat, IBL CO2 cooling flexible transfer line design status, 2013.

[5] Yinshyn Wang, *Fundamental Elements of Applied Superconductivity in Electrical Engineering*.: Wiley, 2013.

[6] S. D. Augustynowicz, J. A. Demko J. E. Fesmire, "Overall Thermal Performance of Flexible Piping Under Simulated Bending Conditions," in *AIP Conference Proceedings 613*, vol. 3, College Park, 2002.

[7] R. C. Duckworth, M. Roden, M. Gouge J. A. Demko, "Testing of a Vacuum Insulated Flexible Line with Flowing Liquid Nitrogen During the Loss of Insulating Vacuum," in *AIP Conference Proceedings 985*, Chattanooga, 2008.

[8] S. D. Augustynowicz, B.E. Scholtens J. E. Fesmire, "Robust Multilayer Insulation for Cryogenics Systems," in *AIP Conference Proceedings 985*, Chattanooga, 2008.

[9] Hiroyasu Yumura, M. Watanabe, Hiroshi Takigawa, Y. Ashibe, Chizuru Suzawa, H. Ito, Masayuki Hirose, Kenichi Sato, Shigeki Isojima, C. Weber, Ron Lee, Jan Moscovic Takato Masuda, "Fabrication and Installation Results for Albany HTS Cable," *IEEE*, vol. 17, no. 2, June 2007.

[10] J. A. Demko, M. L. Roden, J. F. Maguire, C. S. Weber M. J. Gouge, "Vacuum-Insulated, Flexible Cryostats for Long HTS Cables: Requirements, Status and Prospects," in *AIP Conference Proceedings 985*, Chattanooga, 2008.

[11] Nexans Deutschland Industries K. Schippl. Very Low Loss Cryogenic Envelope for Long HTS-Cables.

[12] Ph. Lebrun, P. Rohner H. Laeger, "Long Flexible Transfer Lines for Gaseous and Liquid Helium," *Cryogenics*, vol. 18, pp. 659-662, July 1978.

[13] Christopher Franke, "CO2 Two-Phase Flow Heat Transfer in Minichannels for Detector Cooling at CERN,".

[14] Daniel Helmer, "Investigation of Heat Transfer and Pressure Drop Phenomena of CO2 in Two Phase Flow," Faculty of Mechanical and Process Engineering, University of Applied Science Offenburg, October 6, 2010.

[15] H. Pernegger, "IBL Cooling Requirements," CERN, Geneva, Requirement Document 2011.

[16] CERN. EN/CV Detector Cooling Section. [Online]. http://detector-cooling.web.cern.ch/detector-cooling/data/C6F14_Sat_Curve.htm

[17] S.D. Augustynowicz, J. A. Demko J. E. Fesmire, "Thermal Insulation Performance of Flexible Piping for use in HTS Power Cables," in *AIP Conference Proceedings 613*, College Park, 2002.